Hydrological Sciences Journal

ISSN: (Print) (Online) Journal homepage: https://www.tandfonline.com/loi/thsj20

Hydrology of peat estimated from near-surface water contents

Dimitre D. Dimitrov, Peter Lafleur, Oliver Sonnentag, Julie Talbot & William L. Quinton

To cite this article: Dimitre D. Dimitrov, Peter Lafleur, Oliver Sonnentag, Julie Talbot & William L. Quinton (2022): Hydrology of peat estimated from near-surface water contents, Hydrological Sciences Journal, DOI: 10.1080/02626667.2022.2099281

To link to this article: https://doi.org/10.1080/02626667.2022.2099281

Published online: 12 Aug 2022.

HYDROLOGICAL SCIENCES JOURNAL
https://doi.org/10.1080/02626667.2022.2099281

Hydrology of peat estimated from near-surface water contents

Dimitre D. Dimitrov[a], Peter Lafleur[b], Oliver Sonnentag[c], Julie Talbot[c] and William L. Quinton[d]

[a]Department of University Transfer, Faculty of Arts & Sciences, NorQuest College, Edmonton, AB, Canada; [b]School of the Environment, Trent University, Peterborough, ON, Canada; [c]Département de géographie & Centre d'études nordiques, Université de Montréal, Montréal, QC, Canada; [d]Cold Regions Research Centre, Wilfrid Laurier University, Waterloo, ON, Canada

ABSTRACT

Simple and robust hydrological modelling is critical for peat studies as water content (θ) and water table depth (d_{WT}) are key controls on many biogeochemical processes. We show that near-surface θ can be a good predictor of θ at any depth and/or d_{WT} in peat. This was achieved by further developing the formulae of an existing model and applying it for Mer Bleue bog (Ontario, Canada) and a permafrost peat plateau at Scotty Creek (Northwest Territories, Canada). Simulated θ dynamics at various depths in hummocks and hollows at both sites matched observations with R^2, Willmott's index of agreement (d), and normalized Nash-Sutcliffe efficiency coefficient (NNSE), reaching 0.97, 0.95, and 0.86, respectively. Simulated bog WT dynamics matched observations with R^2, d, and NNSE reaching 0.67, 0.87, and 0.72. Our approach circumvents the difficulties of measuring subsurface hydrology and reveals a perspective for large spatial scale estimation of θ and d_{WT} in peat.

ARTICLE HISTORY
Received 14 November 2021
Accepted 10 June 2022

EDITOR
A. Fiori

ASSOCIATE EDITOR
M. Rahman

KEYWORDS
peatlands; permafrost peat plateaus; near-surface; soil water contents; water table; modelling

1 Introduction

Peatlands are important ecosystems that occupy only ~3% of Earth's surface (Maltby and Immirzi 1993), yet contain large amounts of organic carbon (C), estimated at ~450–500 Pg, i.e. ~1/3 of the world's soil C (Yu 2012, Loisel *et al.* 2014). Therefore, these ecosystems are a primary concern for their potential response to climate change (Yu *et al.* 2003, Fenner and Freeman 2011, Goldstein *et al.* 2020). Moreover, large areas of peatlands are in the zone of permafrost, i.e. ground with a temperature below 0°C for two or more consecutive years (Quinton and Gray 2003), the southern boundary of which is subject to rapid warming and high rates of permafrost thaw, which will ultimately affect their hydrology (Johannessen *et al.* 2004, Jorgenson *et al.* 2010). This vast peatland C store is very sensitive to soil hydrology (Clymo 1983, Lafleur *et al.* 2003), which is a key control on greenhouse gas (GHG) emissions and C sequestration in plants and soil (Bubier *et al.* 2003, Strack *et al.* 2006, Sulman *et al.* 2009). Hence, there is an urgent need to develop better tools for estimating and monitoring peatland hydrology in these remote and diverse ecosystems.

1.1 Challenges with studying hydrology of peat

Peatland hydrology is challenging to study. The reasons for this include: (i) the intrinsic complexity of peat profiles, with sharp transitions between poorly decomposed upper peat of various thickness and large porosity facilitating infiltration and more decomposed waterlogged deeper peat (Holden 2009, Talbot *et al.* 2014, Weber *et al.* 2017); (ii) complex microtopography of peatland surfaces (Shi *et al.* 2015); (iii) pronounced variability of peat properties at microtopographic and mesoscales (Moore *et al.* 2002, Lafleur *et al.* 2005a, 2005b, Sonnentag *et al.* 2008, Dimitrov *et al.* 2010a, 2014); (iv) the presence/absence of ground ice-rich permafrost, which controls the lateral flow, waterlogging and/or water table (WT) depth (Quinton and Baltzer 2013); and (v) influence on heat transfer, and thus freeze/thaw processes (Kurylyk *et al.* 2016, Devoie *et al.* 2019). These challenges impose serious limitations on expensive and spatially scarce field measurements at remote sites.

Ecohydrological modelling offers solutions to some of the issues noted above, but is also challenging. Many models require continuous meteorological drivers at hourly or daily time steps, which often are not measured at the desired locations, and hydrological and soil parameters that may vary widely among sites or even within the same site (Fraser 1999). Examples include saturated hydraulic conductivities that differ vertically and laterally (Reeve *et al.* 2000), evapotranspiration forcing, site aspects and terrain slopes, largely unknown field boundary conditions (Grant 2001), soil water retention curves (SWRCs) with empirical curve-fitted parameters (Mezbahuddin *et al.* 2016), and large, but often unknown, macropore fractions (Baird 1997, Wallage and Holden 2011).

On the other hand, in the past few decades global application of hyperspectral and multispectral airborne and satellite imagery has produced large amounts of spatial data on near-surface soil properties, such as water contents and temperatures at depths of 5 or 10 cm, which can be accessed through websites with application programming interface (API) end points (e.g. OpenWeather n.d., Agro API n.d.). Despite some limitations, such as coarse spatial and temporal resolution with seasonal constraints on image interpretation, difficulties in

CONTACT Dimitre D. Dimitrov dimitre@ualberta.ca NorQuest College, 10215 108 St NW, Edmonton, AB T5J 1L6, Canada

predicting belowground properties and uncertainties in relating imagery directly to ecosystem processes (Arroyo-Mora *et al.* 2018, Kalacska *et al.* 2018), remote sensing data are the only means to assess peatland near-surface hydrological conditions on a large spatial scale. Complemented by ground data collections of plant and soil properties available online through other API websites (e.g. GBIF n.d., Soilgrids REST n.d.), these resources provide an opportunity for large spatial scale simulations through appropriate modelling interfaces, which are currently missing in most process-based models. Hence, given that soil water content (θ) and WT depth (d_{WT}) are key controls on biogeochemical processes in peatlands and that they are difficult to obtain at a large spatial scale, there is an emerging need for robust, but computationally inexpensive, modelling methods. Specifically, models are needed that are applicable at the site (i.e. local) and large spatial (i.e. regional) scales, and that can be driven by easily measurable or accessible hydrological and soil properties for continuous estimation of θ at any depth and/or d_{WT} in peat.

1.2 Rationale of the proposed approach

Dimitrov and Lafleur (2020) proposed a new approach to peatland hydrological modelling, encoded in a simple process-based model named Peat Hydrological Model (PHM), which is now part of a larger online platform for modelling and research named *DIMONA* (©2019 Dimitre Dikov Dimitrov). PHM successfully simulated θ dynamics in peat at various depths by using d_{WT} observations. We propose that the method of Dimitrov and Lafleur (2020) can be developed further to calculate θ at any depth in peat with or without WT measurements. Specifically, their original formulae for calculating peat θ from d_{WT} can be inverted to simulate daily d_{WT} from the observed daily near-surface θ. Further, by inserting the simulated WT ($d_{WT,sim}$) into the original PHM formulae, peat θ at any depth can be simulated.

Since peatlands occur in different climate zones on the globe, it is important that our model is applicable to any climatic setting. In this study we consider two main peatland environments: the low boreal and temperate peatlands and the high-boreal and sub-arctic peat plateaus in the discontinuous permafrost zone. According to Xu *et al.* (2018), these two environments contain the majority of the world's peatlands. The rationale for this research is based upon the premise that the organic soils of peat plateaus are of a similar composition, structure, and porosity to those of non-permafrost low boreal and temperate peatlands (Quinton and Gray 2003, Quinton and Hayashi 2004). The main difference between the two peatland environments is the presence of permafrost in peat plateaus. For consistency throughout this study, the non-permafrost peatlands are referred to hereafter as peatlands and those with permafrost as peat plateaus.

In peat plateaus the permafrost table is the impermeable boundary separating the seasonally thawed (i.e. active) layer and the underlying permafrost, thereby promoting the horizontal runoff. The saturated (thawed) layer and horizontal runoff are all confined to the active layer. The WT, i.e. the upper surface of the zone of saturation where the matric water potential is equal to the atmospheric pressure (Freeze and Cherry 1979), is typically continuous in non-permafrost peatlands and also in peat plateaus during periods of high moisture supply and minimal active layer thaw. However, as the active layer deepens and drains, the WT in peat plateaus can become discontinuous (Wright *et al.* 2009). Figure 1 shows how $d_{WT,}$

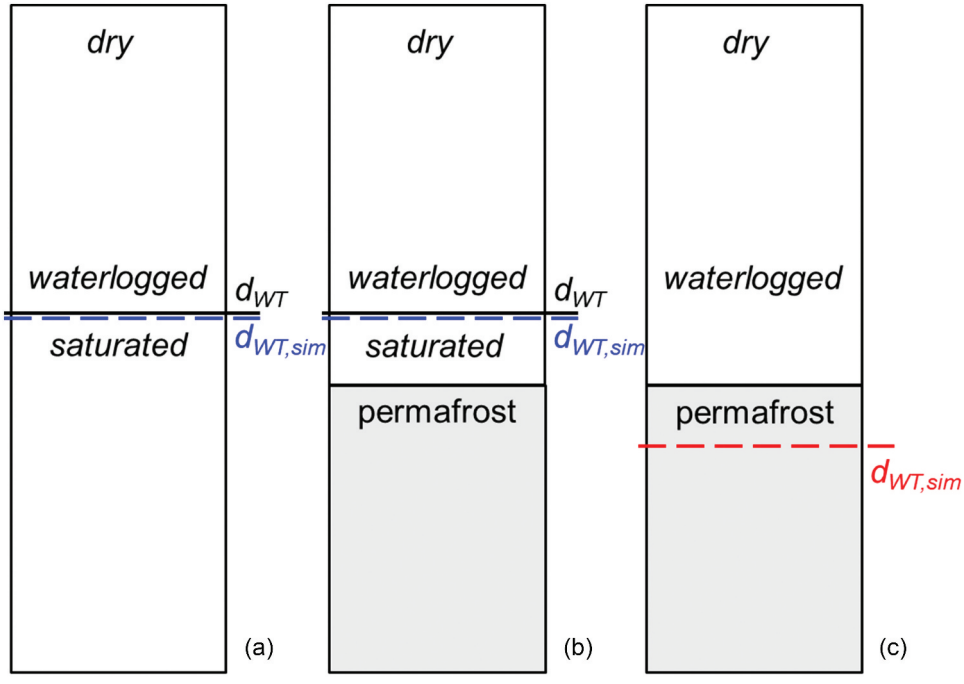

Figure 1. Schematics of (a) a hydrological profile of peat with dry upper and waterlogged deeper layers, observed water table depth (*dWT*), and simulated water table depth (*dWT,sim*) reflecting the observed one in a peatland; (b) a hydrological profile of peat overlying permafrost with dry upper and waterlogged deeper layers, *dWT* and *dWT,sim* reflecting the observed one; and (c) a hydrological profile of peat overlying permafrost with dry upper and waterlogged deeper layers, without *dWT* and *dWT,sim*, reflecting a fictitious water table (i.e. the water table that those peat profiles might have had if permafrost was not present).

$_{sim}$ reflects the existing WT in peatlands (Fig. 1a) or peat plateaus (Fig. 1b), regardless of whether the WT was measured or not.

In the case of no WT in the peat plateau, which cannot be ruled out for some periods of time and locations, $d_{WT,sim}$ in the model reflects a fictitious WT that corresponds to the d_{WT} that those peat profiles might have had if permafrost was not present (Fig. 1c). Simulations of θ with $d_{WT,sim}$ reflecting a fictitious WT are based upon the assumption that daily unsaturated θ in peat plateau profiles are in equilibrium like those in non-permafrost peatlands (Frolking and Crill 1994, Frolking *et al.* 2002). With the uniqueness of the equilibrium state, the daily θ profile above permafrost is expected to be the same as the corresponding θ profile with a fictitious WT in the absence of permafrost. Also, $d_{WT,sim}$ estimated by near-surface θ can reflect the fictitious WT during spring thaw, when the near-surface peat may be thawed, but the majority of the peat profile is still frozen. Thus, by inserting $d_{WT,sim}$ in the original PHM formulae, we can calculate θ at any peat depth with or without permafrost and/or WT observations and at different microforms (hummocks and hollows).

1.3 Objectives and hypotheses

The objectives were to develop novel methods for estimating daily θ (liquid, not ice) at any depth and/or d_{WT} in peat, by using near-surface θ. First we derived formulae for calculating $d_{WT,sim}$ from near-surface θ. We coded these formulae into PHM for dynamic simulation of daily θ at any depth from observed near-surface θ using $d_{WT,sim}$ in the PHM equations of Dimitrov and Lafleur (2020). We then tested the modified PHM for modelling WT and θ at various depths at different microforms of a bog with WT observations and a peat plateau without WT observations. The main hypothesis was that the near-surface θ can be a good predictor of θ at any depth and/or of d_{WT} in peatlands and peat plateaus. The following specific hypotheses were addressed.

Hypothesis 1: The WT depth in peat can be predicted from near-surface θ observations. This hypothesis was tested by inverting the original PHM equations for calculating peat θ at any depth from d_{WT} to calculate daily $d_{WT,sim}$ from the observed near-surface peat θ by log-transformed Campbell and van Genuchten SWRC in PHM. We call this a method for predicting WT (MPWT).

Hypothesis 2: The θ at any depth in a peatland can be predicted from near-surface θ observations. This hypothesis was tested by inserting $d_{WT,sim}$ into the PHM equations to calculate θ at any (user-specified) depth by using the log-transformed Campbell and van Genuchten SWRC.

Hypothesis 3: The θ at any depth in a peat plateau can be predicted from near-surface θ observations. This hypothesis was tested by inserting $d_{WT,sim}$ into the PHM equations to calculate θ at any (user-specified) depth above the permafrost by using the log-transformed Campbell and van Genuchten SWRC. Hypotheses 2 and 3 refer to a method of simulated WT (MSWT).

2 Materials and methods

2.1 Modelling water content profiles using near-surface water contents

2.1.1 Modelling WT using near-surface water contents.

Matric potential in organic soils can be expressed by d_{WT} (m) at a daily time scale (Dimitrov and Lafleur 2020), as follows:

$$\psi_{\mathrm{m,i}} = \frac{-(d_{\mathrm{WT}} - d_{\mathrm{i}})}{100}, \text{therefore } d_{\mathrm{WT}} = 100\left(-\psi_{\mathrm{m,i}}\right) + d_{\mathrm{i}} \tag{1}$$

where $\Psi_{\mathrm{m,i}}$ is the soil matric potential (MPa) at a given depth d_{i} (m) to a soil layer i below the soil surface. Then, by inverting the equations in Dimitrov and Lafleur (2020) for calculating daily volumetric θ_{i} ($\mathrm{m^3\ m^{-3}}$), i.e. $\theta_{\mathrm{i}} = f(\psi_{m,i})$ for log-transformed Campbell and van Genuchten SWRCs, we derived $\psi_{m,i} = f(\theta_{\mathrm{i,obs}})$, which was inserted into Equation (1) to calculate $d_{WT,sim}$ from the observed soil water contents, $\theta_{\mathrm{i,obs}}$, at d_{i}. The general solution for the log-transformed hyperbolic Campbell SWRC and hyperbolic segments of van Genuchten SWRC was:

$$\psi_{\mathrm{m,\,i}} = -e^{\frac{\left\{ln\left(-\psi_{\mathrm{m,\,2}}\right)-\left[ln\left(-\psi_{\mathrm{m,\,2}}\right)-ln\left(-\psi_{\mathrm{m,\,1}}\right)\right]\right\}}{\left\{[ln(\theta_2)-ln(\theta_{\mathrm{i}},obs)]/[ln(\theta_2)-ln(\theta_1)]\right\}}} \tag{2}$$

and the solution for the lowermost segment of van Genuchten SWRC, with properties of an inverse hyperbolic segment, was:

$$\psi_{\mathrm{m,i}} = -e^{\left[\frac{-\left[ln\left(-\psi_{\mathrm{m,\,2}}\right)-ln\left(-\psi_{\mathrm{m,\,1}}\right)\right]M+ln\left(-\psi_{\mathrm{m,\,1}}\right)}{ln(\theta_2)-ln\left(-\psi_{\mathrm{m,\,2}}\right)ln(\theta_1)}\right]/[ln(\theta_2)-ln(\theta_1)]} \tag{3a}$$

$$M = \theta_1/\left[ln\left(-\psi_{\mathrm{m,\,2}}\right) - ln\left(-\psi_{\mathrm{m,\,1}}\right)\right] + 1/\theta_1 + \theta_{\mathrm{i,obs}}/\left[ln\left(-\psi_{\mathrm{m,\,2}}\right) - ln\left(-\psi_{\mathrm{m,\,1}}\right)\right] \tag{3b}$$

where the pairs $\{\theta_1; -\Psi_{\mathrm{m,1}}\}$ and $\{\theta_2; -\Psi_{\mathrm{m,2}}\}$ are the end points of each segment (Fig. 2).

The parameters to substitute for $\{\theta_1; -\Psi_{\mathrm{m,1}}\}$ and $\{\theta_2; -\Psi_{\mathrm{m,2}}\}$ in Equations (2) and (3) for each case above are shown in Fig. 2 at the hygroscopic point (HP), wilting point (WP), field capacity (FC), inflection point (LX), and saturation (sat). Depending on the soil substrate, any of the hyperbolic segments of van Genuchten SWRC could be combined and confined only between the corresponding end points. Thus, van Genuchten SWRC of low inflection point can be confined between the pairs $\{\theta_{\mathrm{r}}; -\Psi_{\mathrm{m,HC}}\}$ and $\{\theta_{\mathrm{LX}}; -\Psi_{\mathrm{m,LX}}\}$ for its hyperbolic part and $\{\theta_{\mathrm{LX}}; -\Psi_{\mathrm{m,LX}}\}$ and $\{\theta_{\mathrm{r}}; -\Psi_{\mathrm{m,HC}}\}$ for its part with properties of the inverse hyperbolic segment (Fig. 2).

The above formulae are used to calculate $d_{WT,sim}$ from $\theta_{\mathrm{i,obs}}$ at a near-surface depth, d_{i}, with Equation (2) or Equation (3), and then the result for $\Psi_{\mathrm{m,i}}$ is inserted into Equation (1). Thus, by choosing d_{i} at near-surface depths (5 or 10 cm, depending on the available data), PHM can simulate the entire range of WT variation within the soil profile at a given site, up to d_{i}.

2.1.2 Modelling water contents at any depth by simulated WT.

Simulated $d_{WT,sim}$ by $\theta_{\mathrm{i,obs}}$ is used by PHM to simulate θ_{i} at any depth of the soil profile specified by the user,

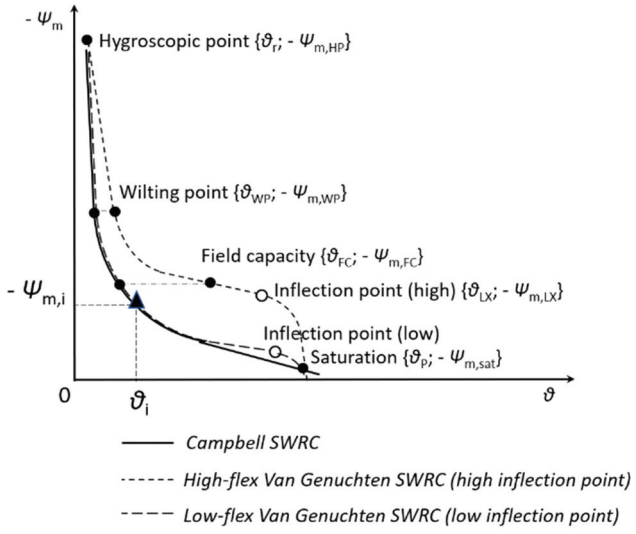

Figure 2. Generalized soil water retention curves (SWRC), hyperbolic Campbell SWRC and sigmoidal van Genuchten SWRC (Dimitrov and Lafleur 2020). The key soil parameters that determine the hyperbolic Campbell SWRC for peat are the pairs {residual soil water content (θr); hydroscopic potential ($-\Psi$m,HC, i.e. the soil matric potential at air-dry condition)} and {total porosity (θp); water potential at saturation ($-\Psi$m,sat)}. The key soil parameters that determine the hyperbolic segments of van Genuchten SWRC in the general case (high inflection point) are the pairs {θr; $-\Psi$m,HC} and {water-filled porosity at wilting point (θWP); water potential at wilting point ($-\Psi$m,WP)} for the upper hyperbolic segment, {θWP; $-\Psi$m,WP} and {water-filled porosity at field capacity (θFC); water potential at field capacity ($-\Psi$m,FC)} for the middle hyperbolic segment, {θFC; $-\Psi$m,FC} and {water-filled porosity at the inflection point (θLX); water potential at the inflection point ($-\Psi$m,LX)} for the lower hyperbolic segment. The lowermost part with properties of the inverse hyperbolic segment is confined between {θLX; $-\Psi$m, LX} and {θr; $-\Psi$m,HC}. Thus, van Genuchten SWRC can be simplified only between {θr; $-\Psi$m,HC} and {θLX; $-\Psi$m,LX} for its hyperbolic part, and {θLX; $-\Psi$m,LX} and {θr; $-\Psi$m,HC} for its other part for both low and high inflection points.

following the relationships $\theta_i = f(\psi_{m,i})$ and $\psi_{m,i} = f(d_{WT})$ described in Dimitrov and Lafleur (2020). Thus, with $\psi_{m,i}$ calculated by $d_{WT,sim}$ in Equation (1), we use the following equations in this study:

$$\theta_i = \left(\frac{\theta_p - \theta_M}{\theta_p}\right)\theta_r^{\left[1-\frac{\ln(-\psi_{m,HC})-\ln(-\psi_{m,i})}{\ln(-\psi_{m,HC})-\ln(-\psi_{m,sat})}\right]}\theta_p^{\left[\frac{\ln(-\psi_{m,HC})-\ln(-\psi_{m,i})}{\ln(-\psi_{m,HC})-\ln(-\psi_{m,sat})}\right]} \quad (4)$$

for the log-transformed Campbell SWRC and

$$\theta_i = \left(\frac{\theta_p - \theta_M}{\theta_p}\right)\theta_r^{\left[1-\frac{\ln(-\psi_{m,HC})-\ln(-\psi_{m,i})}{\ln(-\psi_{m,HC})-\ln(-\psi_{m,LX})}\right]}\theta_{LX}^{\left[\frac{\ln(-\psi_{m,HC})-\ln(-\psi_{m,i})}{\ln(-\psi_{m,HC})-\ln(-\psi_{m,LX})}\right]} \quad (5a)$$

$$\theta_i = \left(\frac{\theta_p - \theta_M}{\theta_p}\right)\left\{\left[\frac{\ln(-\psi_{m,LX})-\ln(-\psi_{m,sat})}{\ln(\theta_{LX})-\ln(\theta_p)}\right]^2\left\{\frac{1}{\theta_{LX}}-\frac{\theta_p^{\left[\frac{\ln(-\psi_{m,i})-\ln(-\psi_{m,LX})}{\ln(-\psi_{m,LX})-\ln(-\psi_{m,sat})}\right]}}{\theta_{LX}^{\left[\frac{\ln(-\psi_{m,i})-\ln(-\psi_{m,sat})}{\ln(-\psi_{m,LX})-\ln(-\psi_{m,sat})}\right]}}\right\}+\theta_{LX}\right\} \quad (5b)$$

for the log-transformed van Genuchten SWRC of two parts only (low or high inflection points). The PHM accounts for macroporosity $\theta_{M,i}$ (m^3 m^{-3}), if any macropore fraction is specified at d_i. Thereby, θ_i is constrained as follows:

$$\theta_i \in [\theta_r; \theta_p) \text{ with } d_{WT} > d_i \text{ and } \theta_i = \theta_p \text{ with } d_{WT} \le d_i \quad (6)$$

2.1.3 Correction for thawing and freezing. Although modelling of soil temperatures at depth is not within the scope of this paper, a general soil temperature function (Jansson 1998, Weiss *et al.* 2006, Wang *et al.* 2020) was introduced in PHM:

$$T_{di} = T_{amean} - T_{aamp}\, e^{-d_i\sqrt{\pi/(D\,y_{cye})}}\cos\left[\frac{(t-t_{ph})(2\pi/y_{cycle})}{-d_i\sqrt{\pi/(D\,y_{cycle})}}\right] \quad (7)$$

where T_{di} (°C) is the soil temperature as a function of the depth d_i and time t (days), T_{amean} (°C) is the annual average soil temperature at d_i, T_{aamp} (°C) is the amplitude (by months) of the soil temperature at d_i, y_{cycle} (days) is the period length, D (m^2 d^{-1}) is the thermal diffusivity of peat, and t_{ph} (days) is the phase shift at d_i, i.e. after how many days thawing/freezing would occur at d_i.

Equation (7) together with Equations (1), (4), (5) and (6) that determine the relationship $\theta_i = f(d_{WT,sim})$ were connected to Equation (8) for implementation in PHM of a new function, f_{TF}, to account for the proper timing of increase and decrease of θ_i at a given depth d_i with thaw and freeze through T_{di} and T_0:

where $\theta_{i,prev}$ is θ_i from the previous day, T_{fpd} (°C) is the freezing point depression, T_B (°C) is the temperature below which further cooling has little effect on θ_i, and T_0 (°C) is the temperature at the soil surface or in the near-surface layer from which d_{WT} is estimated, both calculated with Equation (7).

When the soil surface is thawing and the soil at a depth d_i has not thawed completely, the increase of θ_i (with increase of $d_{WT,sim}$ calculated by increased near-surface θ with thaw) is constrained by Equation (8a), depending on T_{di} and T_0, following the pattern of thawing in a permafrost organic soil (fig. 3b in Quinton and Baltzer 2013). Also, when the soil surface is freezing and the soil at a depth d_i has not frozen completely, the decrease of θ_i (with the decrease of $d_{WT,sim}$ calculated by decreasing near-surface θ with freeze) is maintained by Equation (8b), following the pattern of freezing in a permafrost organic soil (fig. 3a in Quinton and Baltzer 2013). Thus, the changes of θ with thaw and freeze at any depth in PHM are driven by the changes of near-surface θ through Equations (1), (4), (5) and (6), as the timing of θ_i changes at each depth d_i is controlled by f_{TP} through Equation (8) depending on T_{di} and T_0. For simplicity, users can activate f_{TP} only for those soil layers where the timing of θ_i changes with thaw and freeze is expected to be affected by T_{di} and T_0 (e.g. in the deeper waterlogged peat in cold northern regions). In the upper, drier portions of the peat

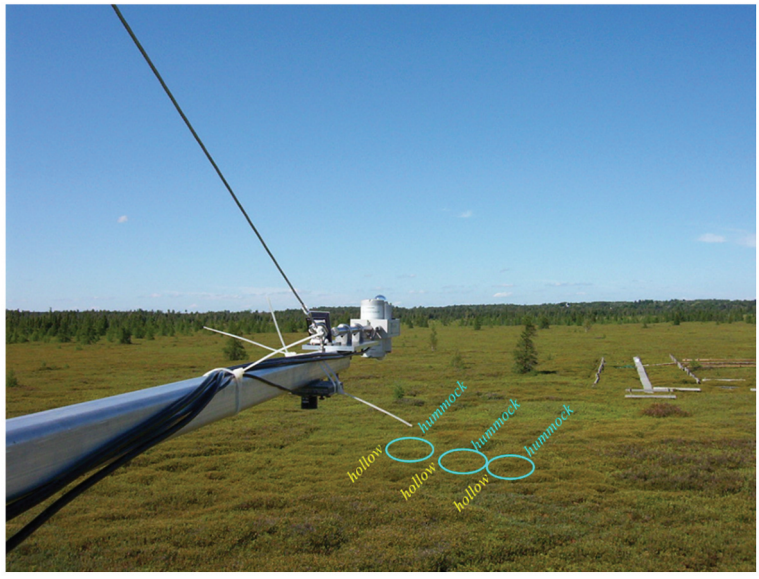

(a)

(b)

Figure 3. Study sites. (a) The hummocky microtopography of Mer Bleue bog, Ontario, Canada. The hummocks of ~1 m diameter occupy about 70% of the surface area, alternating with the hollows that occupy the remaining ~30%, with ~0.25 m between the top of the hummock domes and the hollow surface. (b) The wetland-dominated discontinuous permafrost basin of Scotty Creek, Northwest Territories, Canada. The permafrost peat plateau is the treed area marked by the star (top left), surrounded by open areas of flat bogs and channel fens.

profile, or at lower latitudes with warmer climate, f_{TP} may not be activated, in which case the thaw and freeze changes of θ_i at d_i follow only Equations (1), (4), (5) and (6), i.e. $\theta_i = f(d_{WT,sim})$, and no timing delays with depth are simulated with Equation (8) provided in its two parts below.

$$\theta_i = f_{TP}\left(d_{WT,sim}, T_{di}, T_0\right) =$$

$$= \begin{cases} If\ \ T_0 > T_B = > \begin{cases} f\left(d_{WT,sim}\right) & if\ \ T_{di} \geq 0 \\ max\left\{\theta_{i,prev}; 0.75f\left(d_{WT,sim}\right)\right\} & if\ \ T_{fpd} \leq T_{di} > 0 \\ max\left\{\theta_{i,prev}; 0.5f\left(d_{WT,sim}\right)\right\} & if\ \ T_B \leq T_{di} < T_{fpd} \\ min\left\{\theta_{i,prev}; f\left(d_{WT,sim}\right)\right\} & if\ \ T_{di} < T_B \end{cases} & (8a) \\ If\ \ T_0 \leq T_B = > \begin{cases} \theta_{i,prev} & if\ \ T_{di} \geq 0 \\ max\left\{0.75\theta_{i,prev}; f\left(d_{WT,sim}\right)\right\} & if\ \ T_{fpd} \leq T_{di} > 0 \\ max\left\{0.5\theta_{i,prev}; f\left(d_{WT,sim}\right)\right\} & if\ \ T_B \leq T_{di} < T_{fpd} \\ min\left\{\theta_{i,prev}; f\left(d_{WT,sim}\right)\right\} & if\ \ T_{di} < T_B \end{cases} & (8b) \end{cases}$$

2.1.4 The PHM model. The above formulae were coded into PHM, a simple physically based model built for calculating ambient θ from ambient d_{WT}, and vice versa, based on the specifics of peat SWRC. The model avoids variable soil properties, such as hydraulic conductivities (Fraser 1999) and empirical coefficients of the Campbell and van Genuchten SWRC, by replacing them with hydrological parameters published in the literature (Letts *et al.* 2000, Mezbahuddin *et al.* 2016) or easily measurable on site. PHM now reads daily near-surface θ_{obs} measured on site for the simulation periods. As part of the *DIMONA* platform, PHM can utilize current daily near-surface θ_{obs} and/or soil physical properties at any geographic coordinates in its Internet of Things (IoT) modelling regime, i.e. when near-surface θ_{obs} are provided by websites with API end points, to which PHM is connected through *DIMONA* for real-time simulations (Dimitrov and Lafleur 2021). Although there are no theoretical limitations on the maximum $d_{WT,sim}$, PHM is designed for peat, where WT may vary within the top 1–2 m. PHM does not simulate vertical and lateral soil water fluxes, and hence does not use spatial boundary conditions. Initialization of model simulations for each site starts with the initial records of near-surface θ or d_{WT}, and pre-set parameters of different peat layers for their SWRC, θ_p (from bulk and particle densities), and f_{TP}, measured on site or reported as general peat properties. Model calibration is manual, with parameters varying in ranges, such as $\{\theta_r; \Psi_{m,HC}\}$, $\{\theta_{WP}; \Psi_{m,WP}\}$, $\{\theta_{FC}; \Psi_{m,FC}\}$, $\{\theta_p; \Psi_{m,sat}\}$ and/or $\{\theta_{LX}; \Psi_{m,LX}\}$, θ_M (if any) and t_{ph}.

2.2 Sites and measurements

The performance of PHM was tested at two peatland sites, a non-permafrost bog and a peat plateau, which is a type of bog overlying permafrost. The former is located at Mer Bleue peatland complex, near Ottawa, Ontario, Canada (Lafleur *et al.* 2005a, 2005b), the latter at Scotty Creek research basin, near Fort Simpson, Northwest Territories, Canada (Quinton and Hayashi 2004). Mer Bleue bog (45.41°N, 75.48°W), hereafter referred to as MB (Fig. 3), is one of the most intensively studied peatlands in the world. It has a hummock–hollow microtopography with hummocks representing ~70% and hollows ~30% of the surface area. The hummock tops are elevated ~0.25 m above the hollow bases. The least decomposed, well-drained fibric peat occupies the upper ~0.35 m in hummocks, and the upper ~0.1 m in hollows, followed by a ~0.1 m thick layer of transitional haemic peat across hummocks and hollows. Farther below, the most decomposed, waterlogged sapric peat extends ~4 m down to the contact with mineral soil. d_{WT}, referenced to the hummock surface, was recorded continuously in wells, using a float and counterweight system attached to a potentiometer, complemented by manual d_{WT} measurements to verify the potentiometer readings (Lafleur *et al.* 2005a, 2005b). Daily WT was aggregated from half-hourly measurements in hummocks from 1999 to 2004 and varied from ~0.7 to ~0.25 m below the hummock surface and from ~0 to ~0.5 m below hollows. Daily θ were aggregated from half-hourly measurements at 0.1, 0.2, 0.3, 0.4, and 0.5 m in hummocks, and at 0.03 and 0.15 m in hollows, taken with water content probes (model CS615, Campbell Scientific, Logan, UT). The calibration and normalization of the probes are described by Lafleur *et al.* (2001, 2003, 2005a).

Although the peat plateau at Scotty Creek (61.44°N, 121.25° W), hereafter referred to as SC (Fig. 3), is intensively studied (Quinton *et al.* 2019), there were no WT measurements obtained together with the θ measurements used in this study. θ was measured continuously at 0.05, 0.1, 0.2, 0.3, and 0.4 m below the ground surface in hummocks and hollows with water content probes (model CS615), calibrated by using θ of peat samples collected at the time of installation (Quinton *et al.* 2005). SC has pronounced microtopography, with hummock tops elevated ~0.40 m above hollow bases (Hayness *et al.* 2020). Even if the soil is frozen, there are always residual θ of ~0.2 m^3 m^{-3} in the soil profile (Quinton and Hayashi 2004).

2.3 Model tests and evaluation

2.3.1 Parameterization and simulations for a peatland. To test Hypotheses 1 and 2, PHM was run for MB hummocks and hollows with log-transformed Campbell and van Genuchten SWRC with low inflection point (Table 1) following Dimitrov

Table 1. Summary of PHM model runs with their soil water retention curves (SWRC), model equations implemented in each model run (Equations), sites of model application and model-data comparisons (Site), time series in years for continuous simulations at a daily time step in hummocks and hollows (Period), hypotheses and proposed methods, i.e. Method for Predicting Water Table (MFWT) and Method of Simulated Water Table (MSWT) for predicting soil water contents in peatlands and peat plateaus.

PHM Model Run	SWRC	Equations*	Site	Period	Hypotheses†	Expected Outcome & Purpose
CAMP	Log-transformed Campbell	(1), (2), (4), (6)	Mer Bleue bog	1999 – 2001 hummocks 1999 – 2004 hollows	1, 2	MPWT to model the water table (WT) depth from near-surface soil water contents at a daily time scale.
VANG	Log-transformed Van-Genuchten	(1), (3a,b), (5a,b), (6)	Mer Bleue bog	1999 – 2001 hummocks 1999 – 2004 hollows	1, 2	MSWT to model soil water contents at depth from near-surface soil water contents by simulated WT at a daily time scale in peatlands with or without WT observations.
PLAT	Log-transformed Campbell, Log-transformed Van-Genuchten	(1), (2), (3a,b), (4), (5a,b), (6), (7), (8)	Scotty Creek permafrost peat plateau	2013 – 2019 hummocks and hollows	3	MSWT to model soil water contents at depth from near-surface soil water contents by simulated WT at a daily time scale in peat plateaus with or without WT observations.

*Model equation numbers.
†Hypotheses numbers.

Table 2. Soil model parameters for Mer Bleue bog, hummock and hollow, including soil water retention curves (SWRC), macroporosity (θ_M), total porosity (θ_p), matric potential at saturation (φ_{sat}), residual soil water content (θ_r), hydroscopic potential (i.e. the matric potential in the air-dry condition, φ_{HC}), water content at the inflection point (θ_{LX}), water potential at the inflection point (φ_{LX}), status of the thawing/freezing function (f_{TF}) and its phase shift (t_{ph}). Parameter sources are referenced in detail by Dimitrov and Lafleur (2020).

No Layer [-]	Peat type [-]	Depth of Observation [m]	Layer Thickness [m]	SWRC	θ_M [$m^3\ m^{-3}$]	θ_p [$m^3\ m^{-3}$]	φ_{sat} [MPa]	θ_r [$m^3\ m^{-3}$]	φ_{HC} [MPa]	θ_{LX}* [$m^3\ m^{-3}$]	φ_{LX}* [MPa]	f_{TF}	t_{ph} [days]
					Hummock								
1	Fibric		0 - 0.05	Campbell	0.8	0.93	-0.0007	0.04	-3.1	0.99(θ_p)	-0.00071	Off	-
2		0.1	0.05 - 0.15	&									
3		0.2	0.15 - 0.25	Van Genuchten									
4		0.3	0.25 - 0.35										
5	Hemic	0.4	0.35 - 0.45		0.3	0.88	-0.0007	0.15	-3.1	0.98(θ_p)	-0.00071	Off	-
6	Sapric	0.5	0.45 - 0.55		0	0.83	-0.0007	0.22	-3.1	0.97(θ_p)	-0.00071	Off	-
7- 10			0.55 – 4.0										
					Hollow (~ 25 cm below the hummock surface)								
1	Fibric	0.03	0 - 0.05	Campbell	0.8	0.93	-0.0007	0.04	-3.1	0.99(θ_p)	-0.00071	Off	-
2	Fibric		0.05 - 0.10	&									
3	Hemic	0.15	0.1 - 0.2	Van Genuchten	0.3	0.88	-0.0007	0.15	-3.1	0.98(θ_p)	-0.00071	Off	-
4 - 8	Sapric		0.2 – 3.75										

*Only for Van Genuchten soil water retention curve (SWRC).

and Lafleur (2020). The model run with Campbell SWRC was called CAMP and the one with van Genuchten SWRC was called VANG. CAMP and VANG were driven by observed daily θ at 0.1 m depth during the 1999–2001 period for MB hummocks. Due to a large amount of missing or low-quality observations of θ at 0.1 m during 2002–2004, we did not run PHM for MB hummocks for that period. We used $d_{WT,sim}$ to model θ at depth in MB hummocks. For MB hollows, $d_{WT,sim}$ was the average of the simulated water table using θ at 0.03 and 0.15 m depths, used to avoid effects of evapotranspiration on θ at 0.03 m. The simulations include all years in the 1999–2004 period. CAMP and VANG were parameterized and run for soil profiles of MB hummocks and hollows, consisting of 10 and 8 peat layers , respectively (Table 2), thus capturing the range of WT fluctuations during 1999–2004. General values for peat θ_p and θ_r for the fibric, haemic and sapric peat were taken from Letts *et al.* (2000). The values of $\Psi_{m,sat}$ were taken from the same source; however, they were slightly modified to satisfy $\Psi_{m,sat} = 1/\alpha$, where α is the van Genuchten α parameter in fibric peat, where hydrological changes and θ measurements were most frequent (Mezbahuddin *et al.* 2016). For θ_r we assigned a value of $\Psi_{m,HC}$, i.e. the hydroscopic coefficient (Thien and Graveel 2003). Other parameters in Table 2 were taken from previous modelling studies at MB (see Dimitrov *et al.* 2010a, Dimitrov and Lafleur 2020).

Simulated d_{WT} in hummocks was compared with the corresponding observed WT in hummocks. Field WT in hollows was computed as WT in hummocks minus 0.25 m, i.e. the difference between hummock tops and hollow bases. These values were compared against the simulated WT for hollows. Simulated θ at depths of 0.1, 0.2, 0.3, 0.4, and 0.5 m in hummocks, and 0.03 and 0.15 m in hollows, were compared with the corresponding observed values.

2.3.2 *Parameterization and simulations for a peat plateau.*

To test Hypothesis 3, PHM was run for SC with log-transformed Campbell SWRC for the upper peat and log-transformed van Genuchten SWRC for the deeper peat in hummocks and hollows (Table 1). The PHM run for SC was called PLAT. To avoid effects of near-surface evapotranspiration on θ at 0.05 m, PLAT was driven by the observed daily θ at 0.1 m during the period 2013–2019. The soil profiles at SC hummocks and hollows (Table 3) reflect the field and laboratory measurements at a location representative for both microforms. Observations for bulk density (g cm^{-3}) were taken at each 0.02 m or 0.03 m depth increment from the surface down to 3.46 m depth. Those observations were aggregated into 20 soil layers in PHM. Following Letts *et al.* (2000), a peat type (fibric, haemic, sapric) was assigned to each layer based on its average-weighted bulk density, converted to θ_p using the average-weighted particle density calculated from its organic and mineral contents. Macropore fractions were assigned in hummocks and hollows (Table 3) following Quinton and Hayashi's (2004) report that mean pore diameters decrease from 1580 μm at 3.5 cm depth to 390 μm at 28.5 cm depth. Also, reflected in Tables 3 and 4 are the general pattern of macroporosity decline in hollows with improved contact with water and limited drying, compared to hummocks (Dimitrov *et al.* 2010b).

Two observed SWRCs have been reported for SC (fig. 4 in Quinton and Hayashi 2004), one for the upper 0.1 m peat and another one for the peat between 0.1 and 0.4 m. The shape of the observed SWRC for the upper peat implied low water holding capacity at near-saturation, similar to the observed θ in the upper 30 cm in hummocks and 10 cm in hollows. Therefore, following Dimitrov and Lafleur (2020), we used the log-transformed Campbell SWRC for peat at 0.05, 0.1, 0.2, and 0.3 m in hummocks, and at 0.05 and 0.1 m in hollows. The other observed SWRC, with a more pronounced sigmoidal shape, was considered representative for the deeper peat in hummocks and hollows. Hence, we used the log-transformed van Genuchten SWRC with two parts at 0.4 m in hummocks and 0.2, 0.3, and 0.4 m in hollows. The values of θ_{LX} and $\Psi_{m,LX}$ were inferred from Quinton and Hayashi (2004), and $\Psi_{m,sat}$ was implied from $\Psi_{m,LX}$ (Tables 3 and 4).

Table 3. Soil model parameters for Scotty Creek permafrost peat plateau, hummock and hollow, including soil water retention curves (SWRC), macroporosity (θ_M), total porosity (θ_p), matric potential at saturation (φ_{sat}), residual soil water content (θ_r), hydroscopic potential (i.e. the matric potential at the air-dry condition, φ_{HC}), water content at the inflection point (θ_{LX}), water potential at the inflection point (φ_{LX}), status of the thawing/freezing function (f_{TF}) and its phase shift (t_{ph}). Values for hollow in brackets where different from those for hummock. Parameters from other studies are referenced explicitly in the footnotes.

No Layer [-]	Peat type [-]	Depth of Observation [m]	Layer Thickness [m]	SWRC	θ_M [$m^3\ m^{-3}$]	θ_p [$m^3\ m^{-3}$]	φ_{sat} [MPa]	θ_r [$m^3\ m^{-3}$]	φ_{HC} [MPa]	θ_{LX}* [$m^3\ m^{-3}$]	φ_{LX}* [MPa]	f_{TF}	t_{ph} [days]
Hummock (Hollow, ~ 40 cm below the hummock surface)													
1	Fibric		0 - 0.02	Campbell	0.6 (0.65)	0.9	-0.005	0.2†	-3.1‡	-	-	Off	-
2	Hemic	0.05	0.02 - 0.08										
3	Fibric	0.1	0.08 - 0.12	Campbell	0.6 (0.625)	0.91	-0.005	0.2†	-3.1‡	-	-	Off	-
4	Fibric		0.12 - 0.18										
5	Hemic	0.2	0.18 - 0.22	Campbell (Van Genuchten)	0.6 (0.35)	0.9	-0.005	0.2†	-3.1‡	-(0.6 θ_p)#	-(-0.0055)#	Off	-(40)
6	Sapric		0.22 - 0.28					(0.15)†					
7	Sapric	0.3	0.28 - 0.32	Campbell (Van Genuchten)	0.45 (0.325)	0.85	-0.005	0.2† (0.22)†	-3.1‡	-(0.6 θ_p)#	-(-0.0055)#	Off	-(45)
8	Hemic		0.32 - 0.38										
9	Hemic	0.4	0.38 - 0.42	Van Genuchten	0.3 (0.35)	0.87	-0.005	0.15††	-3.1‡	0.925 θ_p	-0.0055#	On	15
10-20	Hemic &Fibric		0.42 - 3.45							(0.6 θ_p)#	(-0.0055)#		(50)

*Only for Van Genuchten soil water retention curve (SWRC).
†Parameter values by Quinton and Baltzer (2013).
††Parameter values by Letts *et al*. (2000).
‡Parameter values by Thien and Graveel (2003).
#Parameter values by Quinton and Hayashi (2004).

Table 4. Statistics of simulated vs observed daily water table depth (d_{WT}) at Mer Bleue bog, over the periods of 1999 – 2001 for hummocks and 1999 –2004 for hollows. The statistics include the number of observations (N), the coefficient of determination (R^2), slope, intercept Willmott's index of agreement (d), root mean square error (RMSE) with its 95% confidence interval ($CI_{95\%}$), systematic ($RMSE_s$) and unsystematic ($RMSE_u$) components, and the normalized Nash-Sutcliffe efficiency (NNSE) with its $CI_{95\%}$. The negative d_{WT} indicates below the soil surface.

Statistics	N	R^{2*}	Slope*	Intercept*	d	RMSE ($CI_{95\%}$)	$RMSE_s$	$RMSE_u$	NNSE ($CI_{95\%}$)
Units	(-)	(-)	(-)	(cm)	(-)	(cm)	(cm)	(cm)	(-)
Model run with log-transformed Campbell Soil Water Retention Curve, MB_{CAMP}									
Hummock, d_{WT}† cm	545	0.61	0.97	-0.65	0.87	6.7 [5.2; 8.2]	0.8	6.6	0.72 [0.56; 0.81]
Hollow, d_{WT}†† cm	1237	0.67	0.58	-4.5	0.85	10.5 [6.6; 15]	8	6.7	0.55 [0.35; 0.74]
Model run with log-transformed Van Genuchten Soil Water Retention Curve, MB_{VANG}									
Hummock, d_{WT}† cm	545	0.62	1.02	-1.89	0.85	7.1 [5.2; 9.3]	2.6	6.6	0.69 [0.6; 0.77]
Hollow, d_{WT}†† cm	1237	0.67	0.58	-4.5	0.85	10.4 [6.6; 14.9]	7.9	6.7	0.56 [0.36; 0.74]

*From the linear regression of simulations on measurements at significance level $\alpha = 0.05$ ($p < 2.2e\text{-}16$).
†Simulated water table depth (d_{WT}) obtained by using the available near-surface observed soil water contents at depth of 10 cm.
††The average of the simulated water table depth (d_{WT}) obtained by using the available observed soil water contents at depths of 3 and 15 cm.

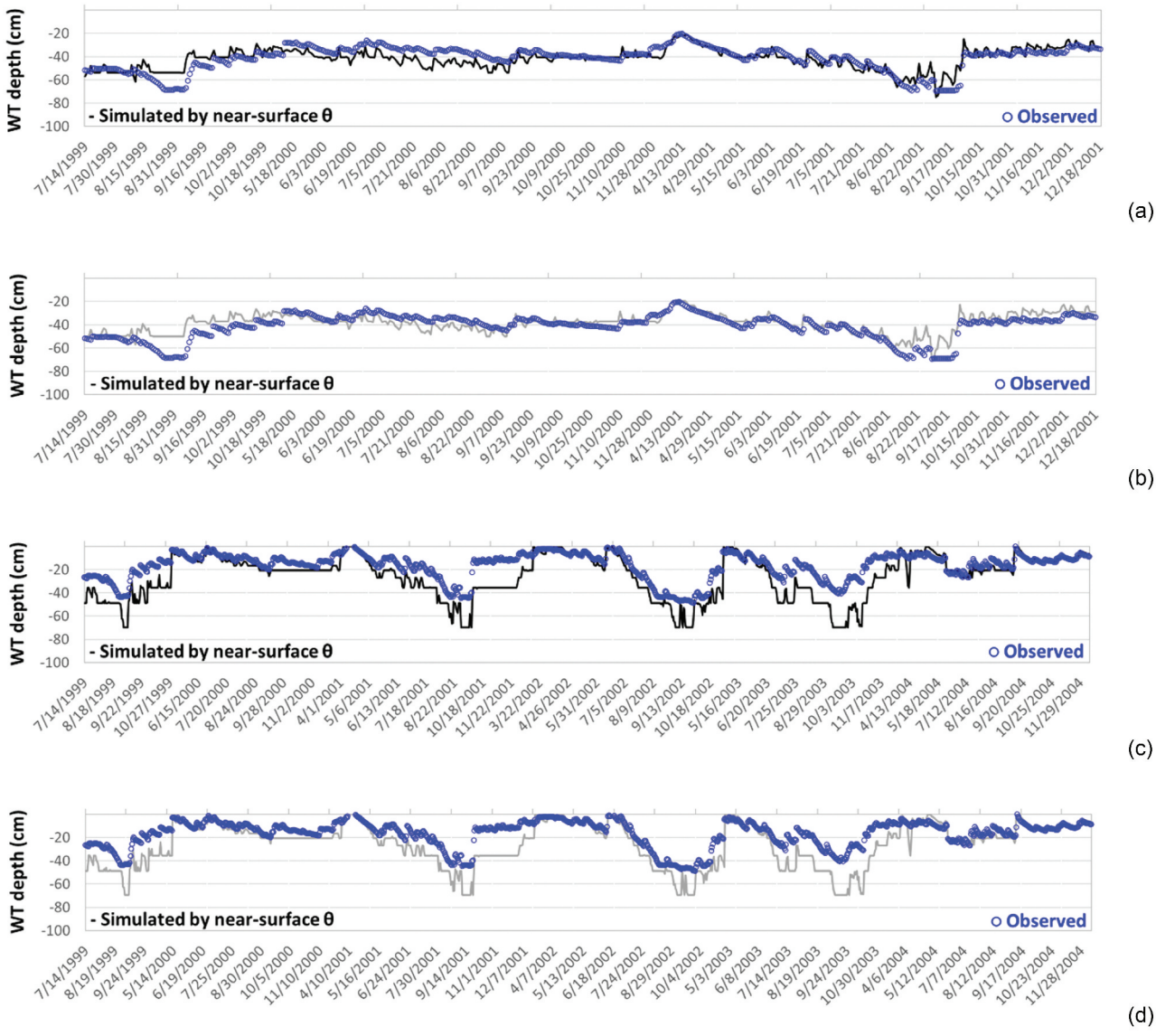

Figure 4. Daily water table (WT) depths at Mer Bleue bog in (a) hummocks, observed and simulated by near-surface soil water contents (θ) and log-transformed Campbell soil water retention curve (SWRC) during the 1999–2001 period; (b) hollows, observed and simulated by near-surface θ and log-transformed Campbell SWRC during the 1999–2004 period; (c) hummocks, observed and simulated by near-surface θ and log-transformed van Genuchten SWRC during the 1999–2001 period; (d) hollows, observed and simulated by near-surface θ and log-transformed van Genuchten SWRC during the 1999–2004 period. The negative vertical scale refers to the depth below the soil surface.

The f_{TF} for seasonal thawing and freezing was applied to the layers at 0.4 m in hummocks and 0.2, 0.3, and 0.4 m in hollows, where these effects were expected to appear with high water contents and waterlogging at depth. The PHM parameters for Equations (7) and (8) were calculated for the entire period of simulations (2013–2019), i.e. T_{amean} = −0.53°C, T_{amean} = 14.27°C, y_{cycle} = 365 days, following Jansson (1991), D = 0.00864 m^2 d^{-1} at SC peat plateau following Braverman (2017), T_B = −0.7°C and T_{fpd} = −0.3°C following Quinton and Baltzer (2013), t-$_{ph}$ = 0 days at surface and user specified for each peat layer (Tables 3 and 4). Simulated θ at depths of 0.05, 0.1, 0.2, 0.3, and 0.4 m in hummocks and hollows were compared with the corresponding observed ones.

2.3.3 Statistical analysis to evaluate model performance. To evaluate PHM performance, linear regressions of simulated d_{WT} and θ (y-axis) on observed d_{WT} and θ (x-axis) were performed at each depth in hummocks and hollows at MB and SC. The overall model accuracy was evaluated using the root mean square error (RMSE) and its systematic (RMSE$_s$) and unsystematic (RMSE$_u$) components (Willmott 1981). Willmott's index of agreement (d, $0 \le d \le 1$) was calculated to estimate the relative model accuracy with respect to the magnitude of observed values (Willmott 1982). The Nash-Sutcliffe efficiency (NSE) coefficient was calculated to assess how well the model performs with respect to the average of the observed values (Krause *et al.* 2005). For convenience, we report the normalized NSE, i.e. NNSE = 1/(2 − NSE), $0 \le$ NNSE ≤ 1 (Nosent and Bauwens 2012). In addition, the 95% confidence

intervals ($CI_{95\%}$) were estimated for RMSE and NNSE by applying the statistical software FITEVAL (Ritter and Munoz-Carpena 2013, 2020).

3 Results

3.1 Modelling WT depth from near-surface θ in a peatland

Both CAMP and VANG closely captured the seasonal and inter-annual dynamics of WT in MB hummocks during the series of dry (1999) – very wet (2000) – dry (2001) years, including the peak WT rise in April 2000 and the development of summer droughts in 1999 and in 2001 (Fig. 4a and b). Also, CAMP and VANG captured the seasonal and inter-annual dynamics of WT in MB hollows during the hydrologically diverse period of dry (1999) – very wet (2000) – dry (2001) – very dry (2002) – normal (2003) – wet (2004) years (Fig. 4c and d). Although for hollows CAMP and VANG often underestimated the observations during the periods of summer WT drawdowns in 1999, 2001, 2002 and 2003, both runs closely followed the observed WT during the wet periods in 1999–2004. Both models also captured the daily WT rise of ~23 cm accompanying the most intensive rain event in that period, 124.5 mm over 24 h on 9 September 2004.

Statistics (observed on modelled) for CAMP and VANG daily d_{WT} in hummocks and hollows of the MB bog are given in Table 4. The R^2 was ~61% for hummocks and 67% for hollows. The slopes were near unity and intercepts near zero for hummocks, while for hollows the slopes departed from unity and intercepts were greater than zero, indicating greater bias in the model compared to hummocks. Willmott's d > 0.85 indicated good model performance of both CAMP and VANG for hummocks and hollows. RMSE values for both runs were smaller and their $CI_{95\%}$ narrower for hummocks compared to those for hollows, but $RMSE_s$ was greater than $RMSE_u$ and approaching RMSE for hollows, suggesting that the parameterization would need improvement rather than the model formulae (Willmott 1981, 1982). The better performance of CAMP and VANG for hummocks was also indicated by their higher NNSE with narrower $CI_{95\%}$, compared to those for hollows. The NNSE and their upper $CI_{95\%}$ boundaries for hummocks reached acceptable values, i.e. NNSE > 0.61 (corresponding to NSE > 0.36 in Ramanarayanan *et al.* 1997, Motovilov *et al.* 1999) and good values, i.e. NNSE > 0.67 (corresponding to NSE > 0.5 in Moriasi *et al.* 2007), NNSE > 0.74 or even > 0.8 (corresponding to NSE > 0.65 or even > 0.8 in Ritter and Munoz-Carpena 2013). The upper $CI_{95\%}$ boundaries of NNSE for hollows indicated acceptable performance for both runs. However, the threshold values for NNSE and NSE given above should be treated with caution for soil hydrology modelling as they were set mainly for large-scale surface hydrology studies (e.g. river or watershed discharge).

3.2 Modelling θ at various depths from near-surface θ in a peatland

The θ simulated by CAMP and VANG followed the seasonal and inter-annual dynamics of observed θ in MB hummocks at all depths (Figs 5 and 6). Both runs captured the dynamics of θ during 1999–2001 in the dry fibric peat in hummocks at 0.1 and 0.2 m, including the two spring thaw peaks in April 2000 and 2001 at 0.2 m. CAMP performed slightly better than VANG at 0.1 m (Figs 4a and 5a) and the two model runs were comparable at the 0.2 m depth (Figs 5b and 6b). Both runs reproduced the magnitude and dynamics of θ changes in the hummock wet fibric peat at 0.3 m with pronounced peaks during spring thaw in April 2000 and 2001 and during intensive rain events in May 2000 (Figs 5c and 6c). Similar results were obtained for the haemic peat at 0.4 m during the summer droughts in 1999 and 2001 and the consistently shallow WT in summer 2000 (Figs 5d and 6d). VANG simulated slightly more waterlogged conditions compared to CAMP at 0.3 and 0.4 m in hummocks. Both runs simulated conditions close to saturation at 0.5 m in hummock sapric peat for most of the time during 1999–2001, and captured the steep declines of θ in August 1999 and September 2001 (Figs 5e and 6e). For hollows, both runs closely captured θ dynamics during the 1999–2004 period at 0.03 and 0.15 m depths (Fig. 7). The thaw and θ peaks between June and July 2000, April and May 2001, April, May and July 2002, and May and June 2003 at 0.03 m were captured too (Fig. 7a and c), as was the summer decline of θ at 0.15 m with droughts in 1999 and 2001 (Fig. 7b and d).

Statistics (observed on modelled) for CAMP and VANG daily θ in MB hummocks and hollows are given in Table 5. Despite the apparent visual fit between simulated and observed θ at 0.2 m in hummocks (Figs 4b and 5b), R^2, slopes, Willmott's d and NNSE were low. However, $RMSE_s$ greater than $RMSE_u$ and approaching RMSE suggests that the parameterization would need improvement rather than the model formulae. Both runs improved their performance in the zone of wet fibric peat at 0.3 m and haemic peat at 0.4 m, where the largest WT fluctuations occurred in hummocks, as reflected by Willmott's d values approaching and surpassing 0.8, and NNSE values and $CI_{95\%}$ boundaries > 0.61 and > 0.74. Although the effect of waterlogging on θ variation at 0.5 m in hummocks made R^2, Willmott's d and NNSE lower compared to those above, the upper NNSE $CI_{95\%}$ boundaries were ~0.61, indicating the potential for acceptable model performance at that depth. Both runs performed well for MB hollows (Table 5).

3.3 Modelling θ at various depths from near-surface θ in a peat plateau

PLAT closely captured the seasonal and inter-annual dynamics of θ at various depths in SC hummocks and hollows during 2013–2019 (Figs 8 and 9). The model was able to simulate θ in the non-saturated upper peat at depths of 0.05, 0.1, 0.2, and 0.3 depths in hummocks (Fig. 8a–d) and 0.05 and 0.1 m in hollows (Fig. 9a and b), and θ in the frequently waterlogged peat at 0.4 m in hummocks (Fig. 8e). Model performance was similar for the depths of 0.2, 0.3, and 0.4 m in hollows (Fig. 9c–e). PLAT captured the pattern of θ increase with spring thaw at the end of April–beginning of May and then the θ decrease with fall freeze at the end of September–October. During the frozen period, between September–October and April–May, PLAT maintained θ at all depths in hummocks and hollows of

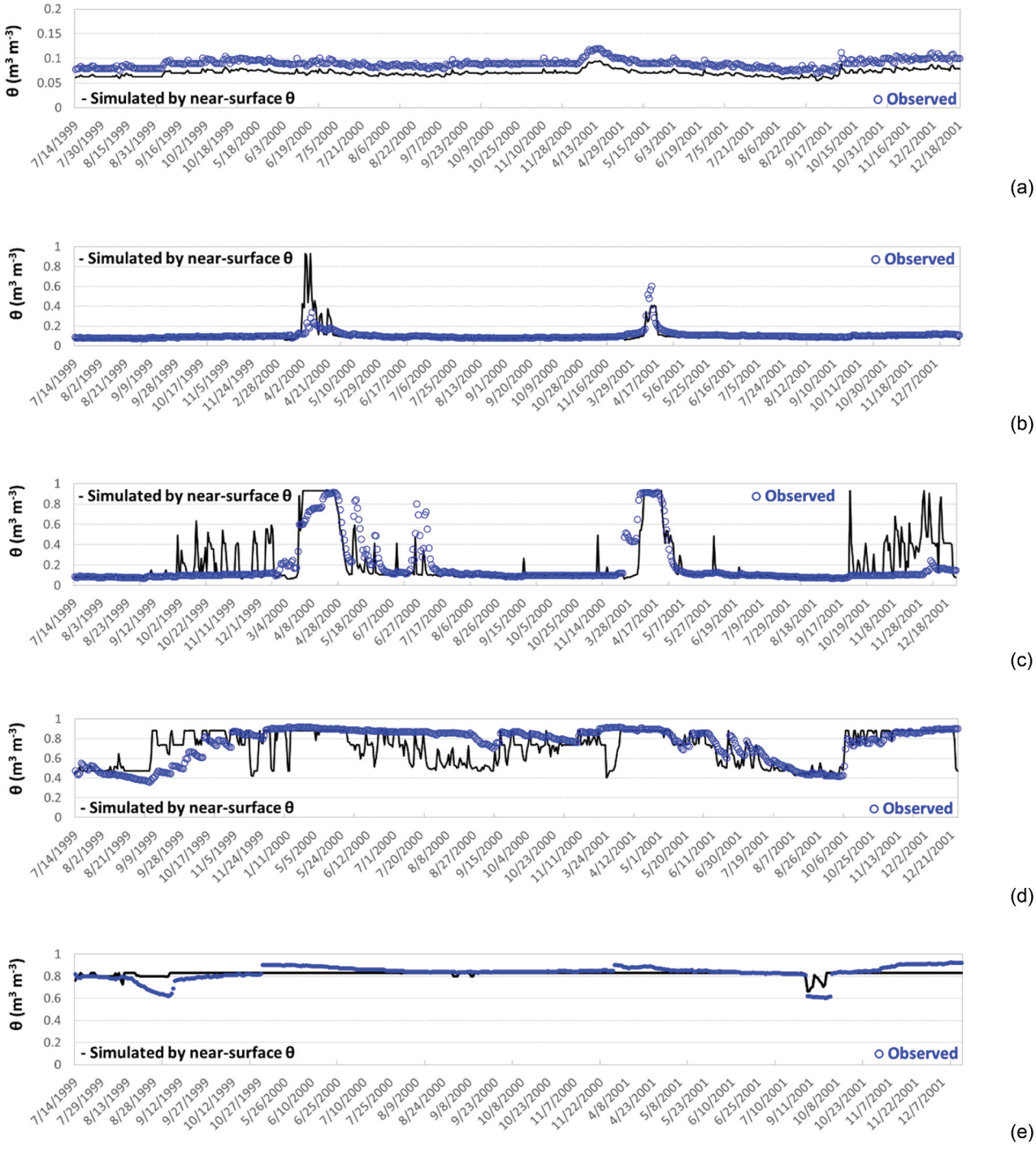

Figure 5. Daily soil water contents (θ) at Mer Bleue bog during the 1999–2001 period in hummocks, observed and simulated by available near-surface θ records and log-transformed Campbell soil water retention curve at depths of (a) 0.1 m, (b) 0.2 m, (c) 0.3 m, (d) 0.4 m, (e) 0.5 m. All depths are with reference to the soil surface (hummock tops).

~0.2–0.3 m^3 m^{-3}, in agreement with the observed residual θ of ~0.2 m^3 m^{-3} at that time of the year (Quinton and Baltzer 2013).

The f_{TF} function for thaw/freeze effects on the timing of simulated θ changes with depth (Tables 3 and 4) was deactivated for PLAT simulations at 0.05, 0.1, 0.2, and 0.3 m in hummocks (Fig. 8a–d), and at 0.05 and 0.1 m in hollows (Fig. 8a and b), due to their low θ and proximity to soil surface. For the deeper peat at 0.4 m in hummocks and at 0.2, 0.3 and 0.4 m in hollows, we compared PLAT with f_{TF} activated and an identical PHM run with f_{TF} deactivated (Figs 8e and 9c–, 9e, respectively). These comparisons demonstrated the importance of thaw/freeze effects on the timing of θ changes with depth. These effects were most pronounced in the waterlogged hollow layers, illustrated by large shifts to the right (later in time) of observed θ at depths of 0.2, 0.3, and 0.4 m due to delayed thaw and freeze at those depths, compared to observed and simulated θ at 0.05 and 0.1 m (Fig. 9c–e). A similar shift of

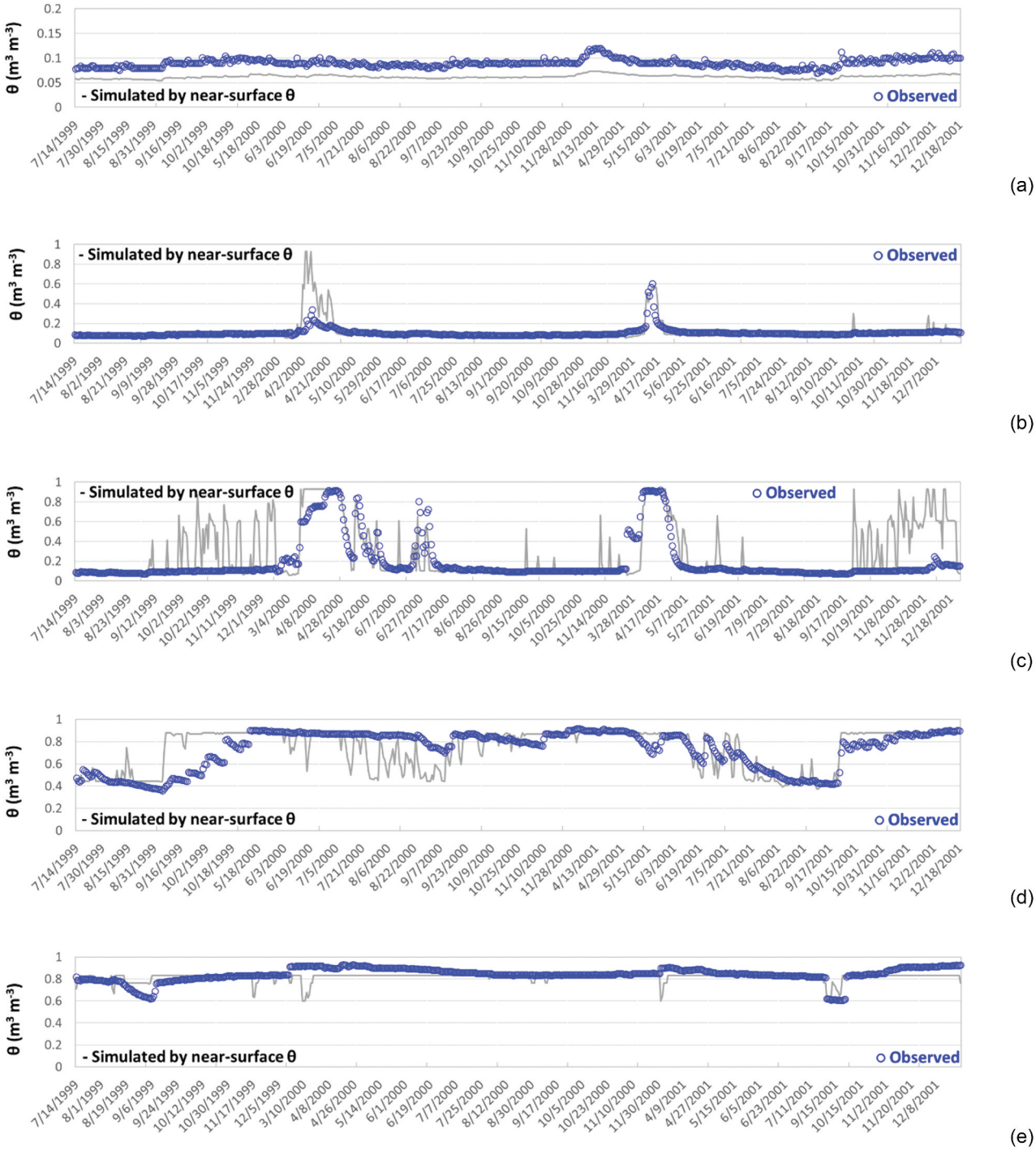

Figure 6. Daily soil water contents (θ) at Mer Bleue bog during the 1999–2001 period in hummocks, observed and simulated by available near-surface θ records and log-transformed van Genuchten soil water retention curve at depths of (a) 0.1 m, (b) 0.2 m, (c) 0.3 m, (d) 0.4 m, (e) 0.5 m. All depths are with reference to the soil surface (hummock tops).

θ to the right was observed at 0.4 m in hummocks, although it was not as large due to the lower θ compared to θ in the waterlogged hollows (Fig. 8e). The lack of thaw/freeze effects on θ in hummocks at 0.05, 0.1, 0.2 and 0.3 m (Fig. 8a–d) can be explained by air convective heat flux that might have occurred in hummocks with heights of ~40 cm (Hayness *et al.* 2020), high porosity and large macropore fractions (Dimitrov *et al.* 2010b). The heat flux enhanced by air convection could have offset T_{di} lagging in depth, hence shifting θ to the right. Therefore, PLAT reproduced the pattern of higher observed θ at 0.05 and 0.1 m compared to those at 0.2, 0.3 and 0.4 m in late April–May in hollows (Fig. 8), which was also evident in hummocks (Fig. 9), and consistent with the field studies at SC (Quinton and Baltzer 2013).

Statistics for PLAT daily θ in SC hummocks and hollows are given in Table 6. Although simulations followed θ observations at 0.05 m (Figs 8a and 9a), the poor statistics at that depth, especially in hollows, can be explained by the evapotranspiration effect on near-surface θ, which is currently not simulated by PHM. For all other depths in both hummocks and hollows,

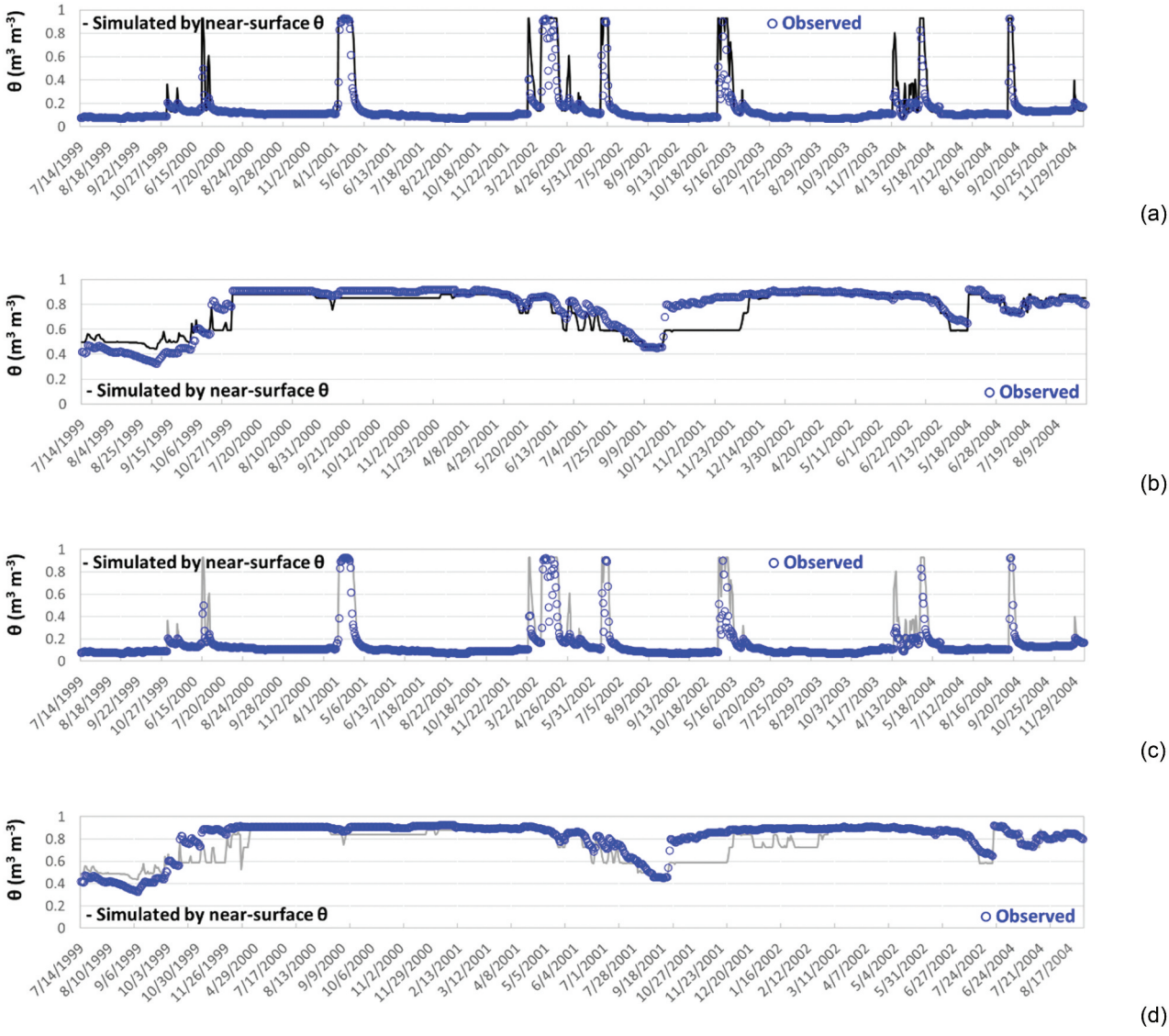

Figure 7. Daily soil water contents (θ) at Mer Bleue bog during 1999–2004 period in hollows at (a) 0.03 m depth, observed and simulated by available near-surface θ records and log-transformed Campbell soil water retention curve (SWRC); (b) 0.15 m depth, observed and simulated by available near-surface θ records and log-transformed Campbell SWRC; (c) 3 cm depth, observed and simulated by available near-surface θ records and log-transformed van Genuchten SWRC; (d) 15 cm depth, observed and simulated by available near-surface θ records and log-transformed van Genuchten SWRC. All depths are with reference to the soil surface (hollow bases). Different time scales are due to reporting simulations only for the corresponding available observations at each depth.

PLAT performed well, demonstrating a good fit between simulated and observed θ. The goodness of fit was confirmed by the high R^2, slopes approaching 1 and intercepts close to 0, small RMSE, Willmott's $d > 0.9$ and NNSE > 0.67 and > 0.74, with their upper $CI_{95\%}$ boundaries > 0.83. When f_{TF} was deactivated for the layers at 0.4 m in hummocks and at 0.2, 0.3, and 0.4 m in hollows, the model performance for those layers degraded, thus confirming statistically the importance of modelling the θ shift with depth caused by seasonal thaw and freeze.

4 Discussion

4.1 Building upon previous modelling work

This study builds upon the previous work of Dimitrov and Lafleur (2020), where PHM was shown to successfully simulate θ at various depths from observed d_{WT} at the MB peatland. PHM has now been further developed to use the near-surface θ_{obs} instead of d_{WT} as a model driver. This modification circumvents the problem that d_{WT} is normally only available at research sites, whereas the near-surface θ can be obtained from other sources at a larger spatial scale (section 1.1). Thus, the near-surface θ_{obs} has been used to drive PHM for modelling $d_{WT,sim}$, which is then used to model θ at any depth. Our findings indicate that both Campbell and van Genuchten SWRCs can be used to model WT dynamics in peat.

Abrupt fluctuations of simulated vs. observed θ at MB (Figs 5–, and 7), especially within the zone of intensive WT variation at 0.3 and 0.4 m in hummocks, might be artefacts of combined sensitivity to near-surface θ_{obs} variation of the exponential Equations (2) and (3) for $d_{WT,sim}$ and exponential Equations (4) and (5) for simulated θ. However, the daily aggregations of near-surface θ_{obs} from API websites may vary less compared to those hourly aggregated on site, thereby mitigating such artefacts. The discrepancy in width between simulated and observed θ below 0.2 m in SC hollows (Fig. 9) could be due

Table 5. Statistics of simulated vs observed daily soil water contents at depths of 0.1 m, 0.2 m, 0.3 m, 0.4 m and 0.5 m in hummocks, and 0.03 m and 0.15 m in hollows at Mer Bleue bog, over the periods of 1999 –2001 for hummocks and 1999 –2004 for hollows. The statistics include the number of observations (*N*), the coefficient of determination (R^2), slope, intercept Willmott's index of agreement (*d*), root mean square error (RMSE) with its 95% confidence interval ($CI_{95\%}$), systematic ($RMSE_s$) and unsystematic ($RMSE_u$) components, and the normalized Nash-Sutcliffe efficiency (NNSE) with its $CI_{95\%}$.

Statistics*	*N*	$R^{2\dagger}$	Slope†	Intercept†	*d*	RMSE ($CI_{95\%}$)	$RMSE_s$	$RMSE_u$	NNSE ($CI_{95\%}$)
Units	(-)	(-)	(-)	($m^3\ m^{-3}$)	(-)	($m^3\ m^{-3}$)	($m^3\ m^{-3}$)	($m^3\ m^{-3}$)	(-)
Model run with log-transformed Campbell Soil Water Retention Curve, MB_{CAMP}									
Hummock, 0.2 m	665	0.37	0.35	0.07	0.69	0.06 [0.02; 0.12]	0.05	0.04	0.34 [0.1; 0.38]
Hummock, 0.3 m	668	0.53	0.66	0.05	0.85	0.17 [0.13; 0.22]	0.08	0.15	0.62 [0.32; 0.78]
Hummock, 0.4 m	632	0.35	0.61	0.32	0.77	0.16 [0.12; 0.2]	0.08	0.13	0.53 [0.32; 0.72]
Hummock, 0.5 m	630	0.09	0.78	0.2	0.41	0.06 [0.05; 0.08]	0.02	0.06	0.51 [0.33; 0.6]
Hollow, 0.03 m	1664	0.79	0.6	0.05	0.9	0.12 [0.09; 0.15]	0.09	0.07	0.63 [0.45; 0.78]
Hollow, 0.15 m	982	0.7	0.91	0.11	0.89	0.1 [0.06; 0.13]	0.05	0.08	0.71 [0.46; 0.87]
Model run with log-transformed Van Genuchten Soil Water Retention Curve, MB_{VANG}									
Hummock, 0.2 m	665	0.5	0.3	0.07	0.68	0.08 [0.03; 0.15]	0.07	0.03	0.24 [0.07; 0.4]
Hummock, 0.3 m	668	0.43	0.5	0.06	0.79	0.23 [0.16; 0.3]	0.16	0.16	0.61 [0.47; 0.72]
Hummock, 0.4 m	632	0.37	0.56	0.34	0.79	0.16 [0.12; 0.2]	0.08	0.13	0.54 [0.36; 0.71]
Hummock, 0.5 m	630	0.14	0.61	0.34	0.54	0.07 [0.05; 0.09]	0.03	0.06	0.48 [0.27; 0.63]
Hollow, 0.03 m	1664	0.79	0.6	0.05	0.9	0.12 [0.09; 0.15]	0.09	0.07	0.63 [0.45; 0.78]
Hollow, 0.15 m	982	0.69	0.9	0.13	0.88	0.1 [0.07; 0.13]	0.05	0.08	0.69 [0.44; 0.86]

*The daily volumetric soil water contents (θ) are modelled at every time step using the simulated water table depths (d_{WT}) from the available near-surface observed θ at depth of 10 cm in hummocks, and by the average simulated d_{WT} from the available observed θ at depth of 3 and 15 cm in hollows.
†From the linear regression of simulations on measurements at significance level $\alpha = 0.05$ ($p < 2.2e\text{-}16$).

to using the general soil temperature function instead of simulating the peat thermal regime (to be implemented in the future). However, for both SWRCs, the PHM performance on modelling θ dynamics in peat profiles driven by the near-surface θ_{obs} (Table 5) was only slightly poorer than the corresponding PHM performance driven by the observed d_{WT} (see table 2 in Dimitrov and Lafleur 2020). The pattern of reported statistics for all θ (Table 5) was consistent with the corresponding pattern in table 2 in Dimitrov and Lafleur (2020), with the best model performance at 0.3 and 0.4 m in hummocks, as well as in hollows, for both SWRCs.

4.2 Advances and uncertainties of the proposed approach

The recent development of PHM has resulted in several methods for modelling peatland hydrology with and without permafrost. Depending on the availability of observed d_{WT} or near-surface θ_{obs}, one can predict WT dynamics alone from near-surface θ_{obs} (Table 1, MPWT), θ dynamics at any depth from near-surface θ_{obs} through $d_{WT,sim}$ (Table 1, MSWT), or θ dynamics at any depth from observed d_{WT}, following Dimitrov and Lafleur (2020). Introducing the f_{TF} function to account for the effects of seasonal thaw/freeze on timing of θ changes at different depths, without explicit simulations of the soil thermal regime, was another important development for modelling hydrology of frozen peat, hence PHM's applicability to a wide variety of soil conditions. By providing an option for users to switch f_{TF} off for layers where the effects of delayed thaw and freeze with depth are not expected, PHM acts to reduce the potential uncertainty with θ simulations in upper peat and warm climate.

Near-surface θ data can be provided by remote sensing at a large spatial scale (Champagne *et al.* 2015, Arroyo-Mora *et al.* 2018). Thus, we anticipate that PHM has the potential to become easily applicable at both site and large spatial scales by utilizing the near-surface θ_{obs} as a model driver. Moreover, PHM has been incorporated recently in the *DIMONA* online platform (sections 1.2 and 2.1.4). *DIMONA* is connected to various websites with API endpoints for providing free 12- or 24-h aggregates of near-surface θ and soil temperatures at 10 cm depth extracted from the remote sensing (OpenWeather n.d., Agro API n.d.), soil profile data for physical and chemical properties, texture, organic C and nutrients down to a depth of 2 m (Soilgrids REST n.d.), and biota (GBIF n.d.), at any geographic coordinates in the world where those data are available (Fig. 10). Hence, using a combination of field data (d_{WT} and/or near-surface θ_{obs} observations and soil physical properties measured at the site), remotely sensed data (near-surface θ_{obs}), and/or website data collections (soil profile properties) to drive PHM and parameterize its soil profiles, it is possible to run simulations in various ways. These include switching from one model driver to another (i.e. from d_{WT} to near-surface θ_{obs} and vice versa), from one site to another, and/or from one site to a series of sites along ecological gradients at a large spatial scale.

Uncertainties with PHM application can arise at the site and large spatial scales. Those at the site scale have been addressed in Dimitrov and Lafleur (2020), and are related to the availability and variability of soil hydrological parameters (e.g. Ψ and θ pairs at various states in Fig. 2), and soil physical parameters (Tables 2, 3 , and 4), with peat type, microtopography, and site category. Reported uncertainties at the large spatial scale are related to the coarse spatial and temporal resolution of remotely sensed data, including the seasonality of their interpretation (Meingast *et al.* 2014, Arroyo-Mora *et al.* 2018, Lees *et al.* 2018). These can affect the estimation of near-surface θ_{obs}, hence its values extracted by remote sensing and/or provided through the request/response cycle via websites with API endpoints (e.g. OpenWeather n.d., Agro API n.d.).

4.3 Implications for remote sensing

PHM could help remote sensing studies by providing a process-based alternative for relating near-surface θ to d_{WT} and/or θ at different depths in the soil profile and expanding these relationships spatially across the landscape. For example, recent remote

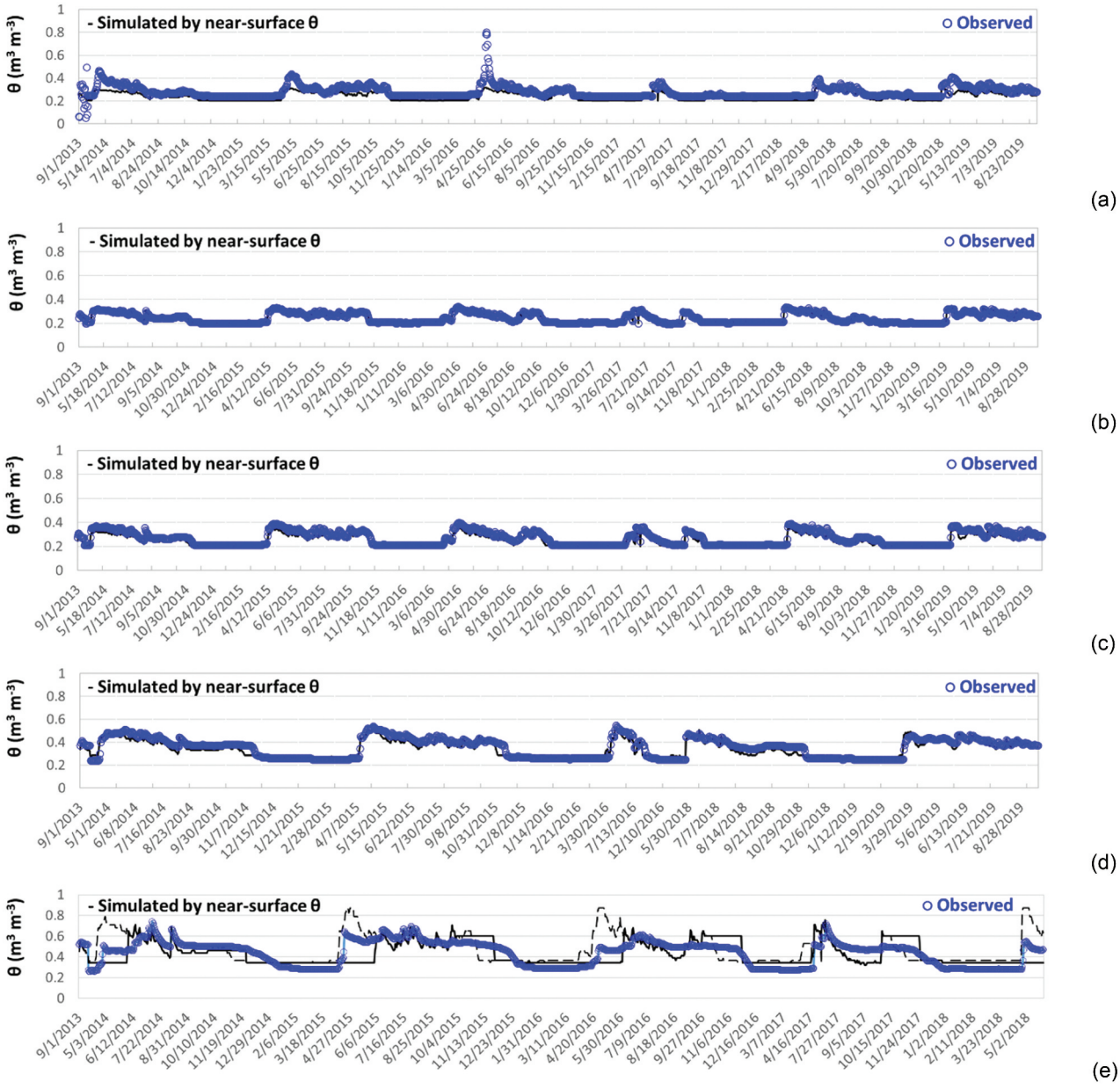

Figure 8. Daily soil water contents (θ) at Scotty Creek permafrost peat plateau during 2013–2019 in hummocks at depths of (a) 0.05 m; (b) 0.1 m; (c) 0.2 m; (d) 0.3 m, observed and simulated by available near-surface θ records and log-transformed Campbell soil water retention curve (SWRC); and (e) 0.4 m, observed and simulated log-transformed van Genuchten SWRC. The dashed line is simulated θ without modelling of the timing of thawing/freezing in wetter peat at 0.4 m depth. All depths are with reference to the soil surface (hummock tops).

sensing studies have empirically related the narrowband $NDWI_{1240}$, i.e. the normalized difference water index (Gao 1996) centred at 1240 nm, to the WT position by simple linear regression (Kalacska *et al.* 2018). This empirical relationship can be replaced by the PHM relationships developed in this study (Table 1), which allow using the near-surface θ extracted by remote sensing to estimate d_{WT} (and/or θ at any depth) and thereby WT intra- and inter-seasonal variation at a landscape scale with variation of surface properties of the landscape. Furthermore, PHM can help remote sensing studies to characterize the hydrology of individual peatlands and peatland complexes, where the remote sensing estimation of near-surface θ is limited mainly to hollows, based on the empirical relationship between $NDWI_{1640}$ and near-surface θ requiring exposed *Sphagnum* cover without seasonal interference from vascular plants (Lalonde 2013, Arroyo-Mora *et al.* 2018). By using the remote sensing near-surface θ in hollows as a model driver, PHM can estimate WT and/or θ at any depth in hollows by $d_{WT,sim}$. Then, based on the interconnectedness of WT between hollows and hummocks, PHM can use $d_{WT,sim}$ adjusted for hummocks by the average hummock minus hollow surface difference for estimating θ at any depth in hummocks.

To demonstrate this concept, we ran PHM for MB during 2002–2004 period with missing near-surface θ_{obs} in hummocks. The hollow $d_{WT,sim}$ was adjusted for hummocks by accounting for the 0.25 m difference between the hummock and hollow surfaces. Thus, the adjusted $d_{WT,sim}$ for hummocks was used to simulate hummock θ at various depths (Fig. 11). Although not as good as the corresponding simulations with observed d_{WT} in hummocks figs 6–9 in Dimitrov

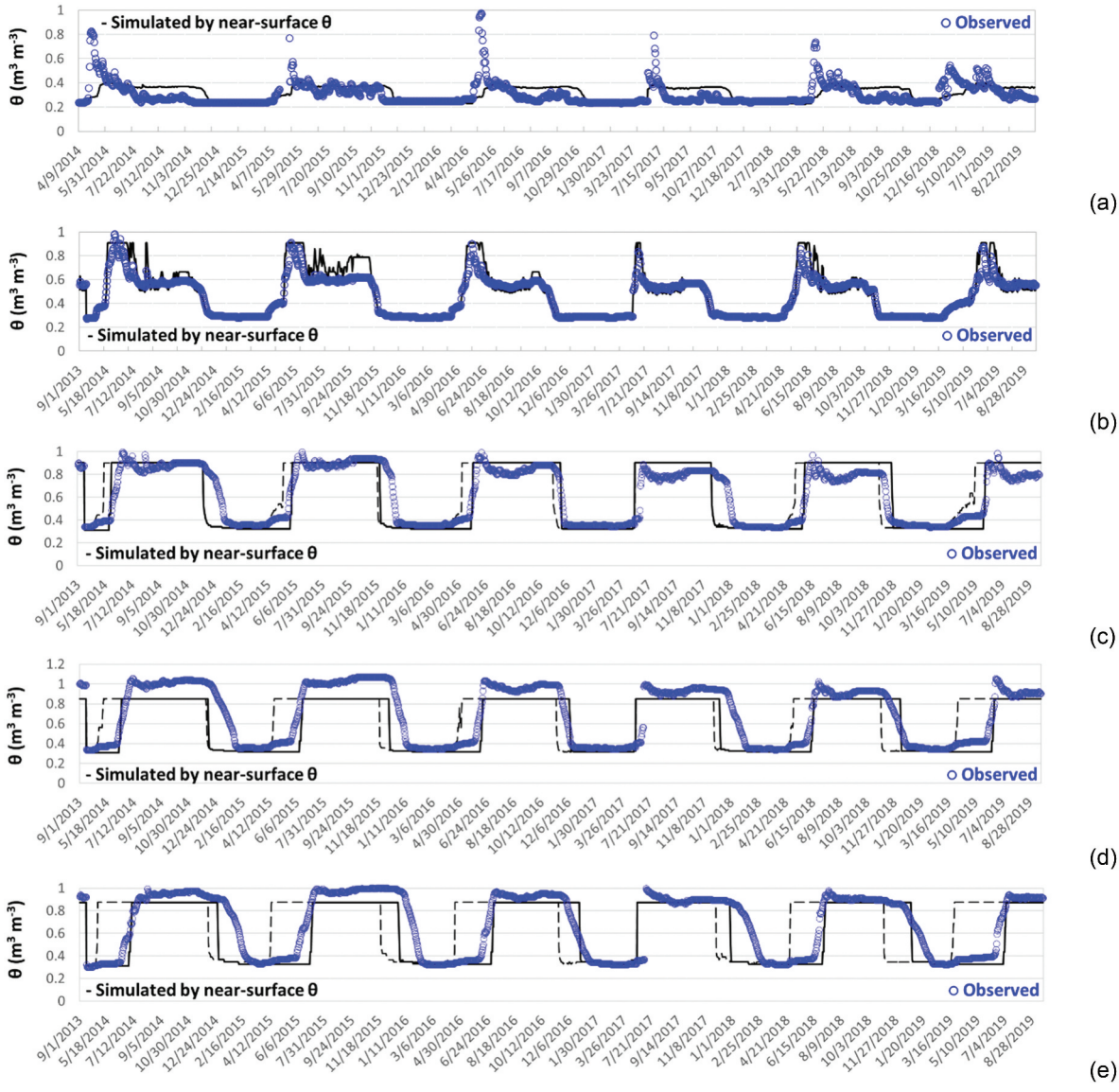

Figure 9. Daily soil water contents (θ) at Scotty Creek peat plateau during 2013–2019 in hollows at depths of (a) 0.05 m; (b) 0.1 m; (c) 0.2 m; (d) 0.3 m, observed and simulated by available near-surface θ records and log-transformed Campbell soil water retention curve (SWRC); and (e) 0.4 m, observed and simulated log-transformed van Genuchten SWRC. The dashed line is simulated θ without modelling of the timing of thawing/freezing in waterlogged peat layers at 0.2, 0.3 and 0.4 m depth. θ values above unity were calibration artefacts of the near-saturation conditions. All depths are with reference to the soil surface (hollow bases).

and Lafleur (2020), PHM with adjusted $d_{WT,sim}$ for hummocks managed to simulate the low θ at 0.2 m (Fig. 11a), captured the pronounced θ dynamics at 0.3 m (Fig. 11b) and 0.4 m (Fig. 11c), and maintained the high θ at 0.5 m (Fig. 11d). Therefore, PHM captured the gross characteristics of the soil water profile.

4.4 Implications for ecosystem modelling

PHM can be applied as an independent hydrological model or coupled to ecological models acting as their hydrological module. As part of *DIMONA*, PHM simulated θ in the peat profile from observed d_{WT}. The simulated θ values at depth were used by *DIMONA* for modelling plant water relations, coupled to photosynthesis and growth of vascular plants and bryophytes. Therefore, PHM provided to *DIMONA* the simulated soil hydrology needed to model the hourly and daily shrub, moss, and ecosystem gross and net primary productivities during a hydrologically diverse period of years (Dimitrov and Lafleur 2021). Additional information on the performance and interface of *DIMONA* online modelling and research platform with PHM can be found at: https://cce-datasharing.gsfc.nasa.gov/files/conference_presentations/Poster_Dimitrov__266_21.pdf. Thus, we show the potential of PHM to be used in ecosystem models as a simple alternative to their sophisticated three-dimensional hydrological schemes and their application for modelling ecological processes.

5 Conclusion

This study supports the main hypothesis that near-surface θ can be used to predict daily θ at any depth in peatlands with and without permafrost, thus revealing a perspective for large spatial scale simulations. New methods have been developed and tested by a simple hydrological model, i.e. for estimating

Table 6. Statistics of simulated vs observed daily soil water contents at depths of 0.1 m, 0.2 m, 0.3 m, 0.4 m and 0.5 m in hummocks, and 0.03 m and 0.15 m in hollows at Scotty Creek permafrost peat plateau over 2013 – 2019 period. The statistics include the number of observations (N), the coefficient of determination (R^2), slope, intercept Willmott's index of agreement (d), root mean square error (RMSE) with its 95% confidence interval ($CI_{95\%}$), systematic ($RMSE_s$) and unsystematic ($RMSE_u$) components, and the normalized Nash-Sutcliffe efficiency (NNSE) with its $CI_{95\%}$.

*Statistics	N	$R^{2\dagger}$	Slope†	Intercept†	d	RMSE ($CI_{95\%}$)	$RMSE_s$	$RMSE_u$	NNSE ($CI_{95\%}$)
Units	(-)	(-)	(-)	($m^3\ m^{-3}$)	(-)	($m^3\ m^{-3}$)	($m^3\ m^{-3}$)	($m^3\ m^{-3}$)	(-)
Model run with layer-specific log-transformed Campbell (predominantly) or Van Genuchten Soil Water Retention Curve, SC									
Hummock, 0.05 m	1814	0.63	1.2	0	0.69	0.05 [0.04; 0.07]	0.04	0.03	0.5 [0.46; 0.52]
Hummock, 0.2 m	1949	0.97	1.26	-0.04	0.93	0.03 [0.02; 0.03]	0.04	0.07	0.81 [0.77; 0.85]
Hummock, 0.3 m	1316	0.87	1.13	-0.03	0.95	0.03 [0.03; 0.04]	0.02	0.03	0.86 [0.79; 0.9]
Hummock, 0.4 m	1425	0.33	0.5	0.2	0.73	0.12 [0.1; 0.15]	0.08	0.1	0.52 [0.49; 0.6]
Hummock*, 0.4 m	1425	0.48	0.73	0.12	0.83	0.09 [0.08; 0.11]	0.03	0.08	0.63 [0.54; 0.71]
Hollow, 0.05 m	1798	0.07	0.48	0.16	0.45	0.12 [0.08; 0.18]	0.03	0.12	0.5 [0.47; 0.53]
Hollow, 0.2 m	1949	0.61	0.68	0.19	0.88	0.17 [0.15; 0.2]	0.09	0.15	0.65 [0.59; 0.73]
Hollow*, 0.2 m	1949	0.78	0.73	0.17	0.93	0.14 [0.11; 0.17]	0.08	0.11	0.75 [0.66; 0.83]
Hollow, 0.3 m	1949	0.37	0.69	0.26	0.79	0.25 [0.21; 0.29]	0.1	0.23	0.57 [0.5; 0.65]
Hollow*, 0.3 m	1949	0.79	0.96	0.13	0.91	0.17 [0.13; 0.22]	0.11	0.13	0.74 [0.64; 0.83]
Hollow, 0.4 m	1949	0.13	0.39	0.42	0.67	0.3 [0.25; 0.34]	0.16	0.25	0.56 [0.39; 0.64]
Hollow*, 0.4 m	1949	0.75	0.86	0.16	0.91	0.16 [0.13; 0.2]	0.09	0.14	0.74 [0.64; 0.83]

*The daily volumetric soil water contents (θ) are modelled at every time step using the simulated water table depths (d_{WT}) from the available near-surface observed θ at depth of 10 cm in hummocks, and hollows.

†From the linear regression of simulations on measurements at significance level $\alpha = 0.05$ ($p < 2.2e\text{-}16$).

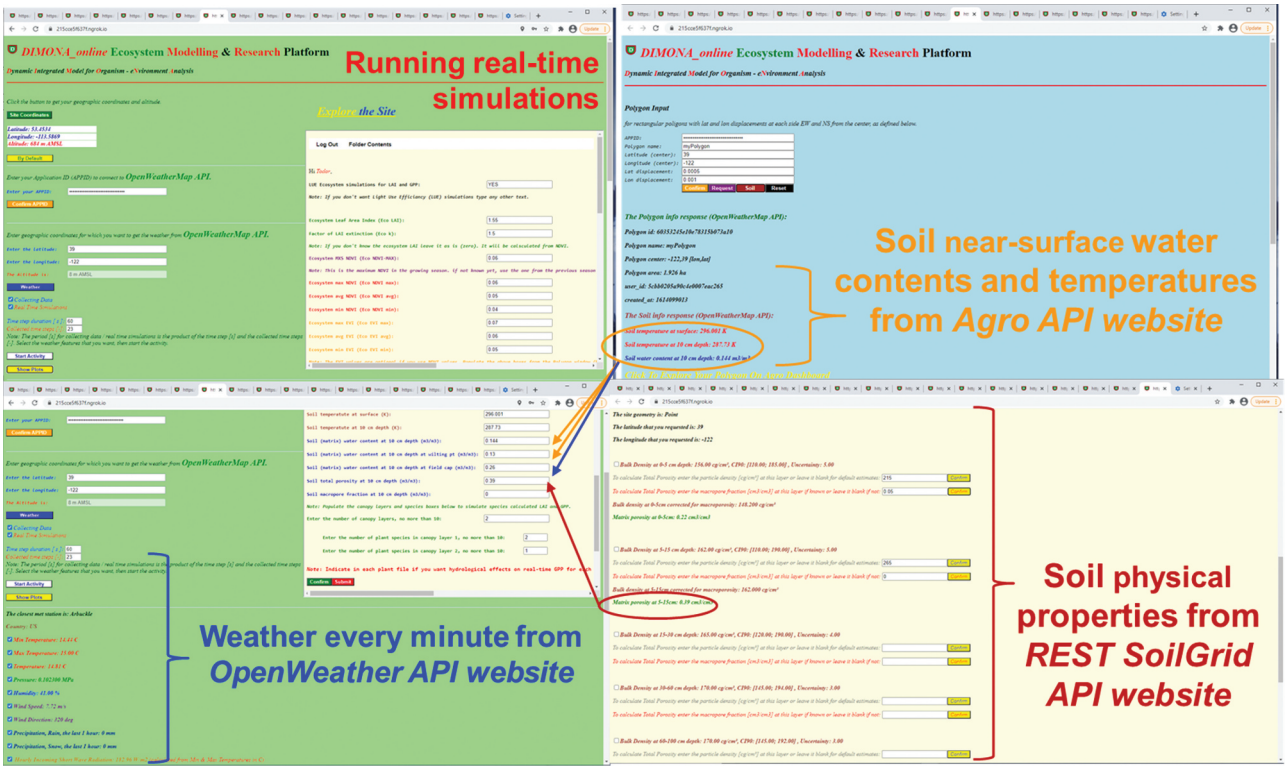

Figure 10. The 12-hour near-surface soil water contents and soil temperatures at 10 cm depth, soil physical properties down to 2m depth below the ground surface, and weather inputs at a one-minute time step, at a shrub site near Sacramento (California, US) with geographic coordinates 39°N and 122°W, requested by *DIMONA* online modelling and research platform, to which PHM is embedded, and received in response from Agro API website, REST SoilGrid website, and OpenWeather website, for real time simulations of shrub productivity controlled by ambient hydrology, with application programming interface (API) endpoints (Dimitrov and Lafleur 2021).

WT from near-surface θ in peat (Hypothesis 1), and for estimating θ at any depth from simulated WT by near-surface θ in peatlands (Hypothesis 2) and on peat plateaus (Hypothesis 3). The methods and the model can be applied at any location for which there are near-surface θ records and soil physical properties, measured on site, reported in the literature, provided on the Internet, or extracted by remote sensing. The simulations can be implemented by embedding the model into an online modelling and research platform, which requests and obtains from various API websites the near-surface daily θ and soil physical properties for any geographic coordinates in the world, thereby providing an opportunity to upgrade from site to large spatial scale modelling. These new methods can enhance remote sensing

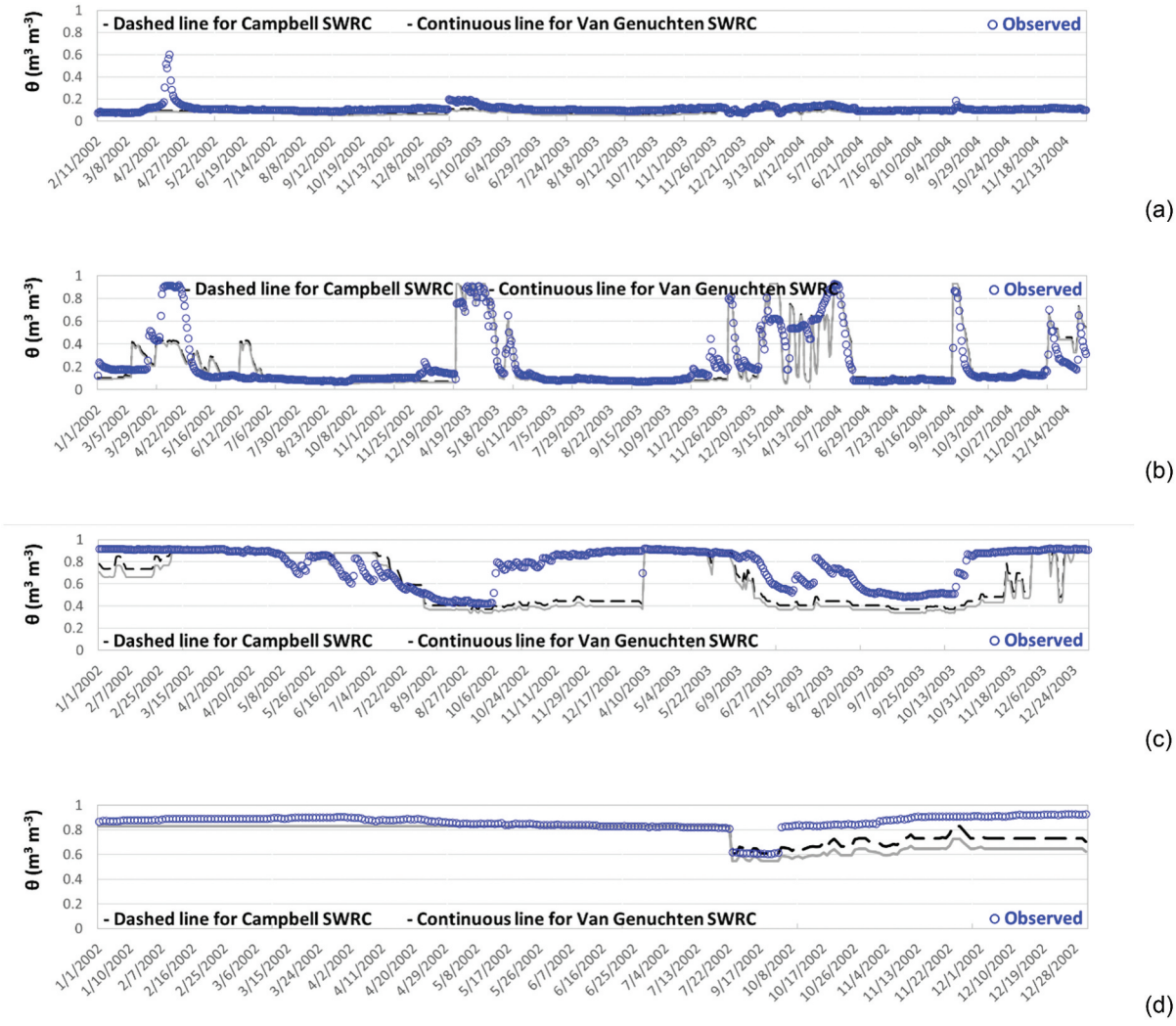

Figure 11. Daily soil water contents (θ) at Mer Bleue bog during the 2002–2004 period in hummocks, observed and simulated at depths of (a) 0.2 m, (c) 0.3 m, (d) 0.4 m, (e) 0.5 m. Simulations were driven by available near-surface θ records at the adjacent hollows by applying the log-transformed Campbell and van Genuchten soil water retention curves (SWRC), and by correcting the simulated water table (WT) depth in hollows for the average difference of ~0.25 m between the hummock tops and hollow bases to represent simulated WT depth in hummocks. The latter was used to estimate the hummock θ at the above depths. All depths are with reference to the hummock tops.

studies by providing a process-based alternative to their regression-based relationships between near-surface properties and hydrology of peat. The approach proposed in this study can improve our understanding, estimation, and dynamic simulation of peatland hydrology at large spatial scales where field observations are absent.

Acknowledgements

Field and lab data were collected with funding from Canadian Carbon Program and Fluxnet Canada Research Network, Natural Sciences and Engineering Council of Canada (NSERC), Canadian Foundation for Climate and Atmospheric Sciences, BIOCAP Canada, Canada Research Chairs, Canada Foundation for Innovation Leaders Opportunity Fund, ArcticNet, and with the support of Liidlii Kue and Jean-Marie River First Nations. The authors are thankful to Mr Gabriel Gosselin and Ms Maude Auclair for their technical assistance in preparing the data.

Disclosure statement

No potential conflict of interest was reported by the authors.

References

Agro API, n.d. Available from: https://agromonitoring.com/

Arroyo-Mora, J., et al., 2018. Airborne hyperspectral evaluation of maximum gross photosynthesis, gravimetric water content, and CO2 uptake efficiency of the Mer Bleue ombrotrophic Peatland. *Remote Sensing*, 10 (4), 565. doi:10.3390/rs10040565

Baird, A.J., 1997. Field estimation of macropore functioning and surface hydraulic conductivity in a fen peat. *Hydrological Processes*, 11 (3), 287–295. doi:10.1002/(SICI)1099-1085(19970315)11:3<287::AID-HYP443>3.0.CO;2-L

Braverman, M., 2017. Impact of linear disturbances on a discontinuous Permafrost Peatland Environment. *Theses and Dissertations (Comprehensive)*, 1915. https://scholars.wlu.ca/etd/1915

Bubier, J., et al., 2003. Spatial and temporal variability in growing season net ecosystem carbon dioxide exchange at a large peatland in Ontario, Canada. *Ecosystems*, 6, 353–367.

Champagne, C., et al., 2015. Satellite surface soil moisture from SMOS and Aquarius: assessment for applications in agricultural landscapes. *International Journal of Applied Earth Observation and Geoinformation*, 45 (B), 143–154. doi:10.1016/j.jag.2015.09.004

Clymo, R.S., 1983. Peat. In: A.J.P. Gore, ed. *Ecosystems of the World*. Mires: Swamp, Bog, Fen and Moor General Studies, Elsevier, NY, Vol. 4A, 159–224.

Devoie, E.G. et al., 2019. Taliks: a tipping point in discontinuous permafrost degradation in peatlands. *Water Resources Research*, 55 (11), 9838–9857. doi:10.1029/2018WR024488

Dimitrov, D.D., et al., 2010a. Modelling subsurface hydrology of Mer Bleue bog. *Soil Science Society of America Journal*, 74 (2), 680–694. doi:10.2136/sssaj2009.0148

Dimitrov, D.D., et al., 2010b. Modelling the effects of hydrology on ecosystem respiration at Mer Bleue bog. *Journal of Geophysical Research - Biogeosciences*, 115 (G4), G04043. doi:10.1029/2010JG001312

Dimitrov, D.D., Bhatti, J.S., and Grant, R.F., 2014. The transition zones (ecotone) between boreal forests and peatlands: ecological controls on ecosystem productivity along a transition zone between upland black spruce forest and a poor forested fen in central Saskatchewan. *Ecological Modelling*, 291, 96–108. doi:10.1016/j.ecolmodel.2014.07.020

Dimitrov, D.D. and Lafleur, P.M., 2020. Revisiting water retention curves for simple hydrological modelling of peat. *Hydrological Sciences Journal*, doi:10.1080/02626667.2020.1853132

Dimitrov, D.D. and Lafleur, P.M., 2021. From ecological models to modelling platforms: bridging science, scientific programming, and web application development. (*poster*) 7th Open Science Meeting, North American Caron Program (NACP), March 2021, Session Linkages among the Air-Land-Water Continuum.https://cce-datasharing.gsfc.nasa.gov/files/conference_presentations/Poster_Dimitrov__266_21.pdf

Fenner, N. and Freeman, C., 2011. Drought-induced carbon loss in peatlands. *Nature Geoscience*, 4 (12), 895–900. doi:10.1038/ngeo1323

Fraser, C.J.D., 1999. *The hydrology and dissolved organic carbon (DOC) biogeochemistry in a boreal peatland*. Thesis (MSc), McGill University.

Freeze, R.A. and Cherry, J.A., 1979. *Groundwater*. 9780133653120. OCLC 252025686. Englewood Cliffs, NJ: Prentice-Hall.

Frolking, S. and Crill, P.M., 1994. Climate controls on temporal variability of methane flux from a poor fen in southeastern New Hampshire: measurement and modeling. *Global Biogeochemical Cycles*, 8 (4), 385–397. doi:10.1029/94GB01839

Frolking, S., et al., 2002. Modelling the seasonal to annual carbon balance of Mer Bleue bog, Ontario, Canada. *Global Biogeochemical Cycles*, 16 (3), 1030. doi:10.1029/2001GB001457

Gao, B.-C., 1996. NDWI – a normalized difference water index for remote sensing of vegetation liquid water from space. *Remote Sensing of Environment*, 58 (3), 257–266. doi:10.1016/S0034-4257(96)00067-3

GBIF, n.d. Available from: https://www.gbif.org/

Goldstein, A., et al., 2020. Protecting irrecoverable carbon in Earth's ecosystems. *Nature Climate Change*, 10 (4), 287–295. doi:10.1038/s41558-020-0738-8

Grant, R.F., 2001. A review of the Canadian ecosystem model ECOSYS. In: M. Shaffer, ed. *Modeling carbon and nitrogen dynamics for soil management*. Boca Raton, FL: CRC Press, 173–264.

Hayness, K.M., et al., 2020. The role of hummocks in re-establishing black spruce forest following permafrost thaw. *Ecohydrology*, 14 (3), e2273. doi:10.1002/eco.2273

Holden, J., 2009. Flow through macropores of different size classes in blanket peat. *Journal of Hydrology*, 364 (3 – 4), 342–348. doi:10.1016/j.jhydrol.2008.11.010

Jansson, P.-E., 1991. *Simulation Model for soil water and heat conditions*. Swedish University of Agricultural Sciences, Uppsala, Report 165.

Jansson, P.-E., 1998. *Simulating model for soil water and heat conditions. Description of the SOIL model. Swedish*. Uppsala, : University of Agricultural Sciences, 0282–6569.

Johannessen, O.M., et al., 2004. Arctic climate change: observed and modelled temperature and sea-ice variability. *Tellus Series A: Dynamic Meteorology and Oceanography*, 56 (4), 328–341. doi:10.3402/tellusa.v56i4.14418

Jorgenson, M.T., et al., 2010. Resilience and vulnerability of permafrost to climate change. *Canadian Journal for Forest Research*, 40 (7), 1219–1236. doi:10.1139/X10-060

Kalacska, M., et al., 2018. Estimating peatland water table depth and net ecosystem exchange: a comparison between satellite and airborne imagery. *Remote Sensing*, 10(5), 687. License. CC BY 4.0. doi:10.3390/rs10050687.

Krause, P., Boyle, D.P., and Base, F., 2005. Comparison of different efficiency criteria for hydrological model assessment. *Advances in Geosciences*, 5, 89–97. doi:10.5194/adgeo-5-89-2005

Kurylyk, B.L., et al., 2016. Influence of vertical and lateral heat transfer on permafrost thaw, peatland landscape transition, and groundwater flow. *Water Resources Research*, 52 (2), 1286–1305. doi:10.1002/2015WR018057

Lafleur, P.M., Roulet, N.T., and Admiral, S.W., 2001. Annual cycle of CO 2 exchange at a bog peatland. *Journal of Geophysical Research*, 106 (D3), 3071–3081. doi:10.1029/2000JD900588

Lafleur, P.M., et al., 2003. Interannual variability in the peatland-atmosphere carbon dioxide exchange at an ombrotrophic bog. *Global Biogeochemical Cycles*, 17 (2), 1036. doi:10.1029/2002GB001983

Lafleur, P.M., et al., 2005a. Ecosystem respiration in a cool temperate bog depends on peat temperature but not on water table. *Ecosystems*, 8 (6), 619–629. doi:10.1007/s10021-003-0131-2

Lafleur, P.M., et al., 2005b. Annual and seasonal variability in evapotranspiration and water table at a shrub-covered bog in southern Ontario, Canada. *Hydrological Processes*, 19 (18), 3533–3550. doi:10.1002/hyp.5842

Lalonde, M., 2013. The Hyperspectral Determination of Sphagnum Water Content in a Bog. Master's Thesis, McGill University, Montreal, QC, Canada.

Lees, K.J., et al., 2018. Potential for using remote sensing to estimate carbon fluxes across northern peatlands – a review. *Science of the Total Environment*, 615, 857–874. doi:10.1016/j.scitotenv.2017.09.103

Letts, M.G., et al., 2000. Parametrization of peatland hydraulic properties for the Canadian land surface scheme. *Atmosphere-Ocean*, 38 (1), 141–160. doi:10.1080/07055900.2000.9649643

Loisel, J., et al., 2014. A database and synthesis of northern peatland soil properties and Holocene carbon and nitrogen accumulation. *The Holocene*, 24 (9), 1028–1042. doi:10.1177/0959683614538073

Maltby, E. and Immirzi, P., 1993. Carbon dynamics in peatlands and other wetland soils regional and global perspectives. *Chemosphere*, 27 (6), 999–1023. doi:10.1016/0045-6535(93)90065-D

Meingast, K.M., et al., 2014. Spectral detection of near-surface moisture content and water-table position in northern peatland ecosystems. *Remote Sensing of Environment*, 152, 536–546. doi:10.1016/j.rse.2014.07.014

Mezbahuddin, M., Grant, R.F., and Flanagan, L.B., 2016. Modelling hydrological controls on variations in peat water content, water table depth, and surface energy exchange of a boreal Western Canadian fen peatland. *Journal of Geophysical Research - Biogeosciences*, 121 (8), 2216–2242. doi:10.1002/2016JG003501

Moore, T.R., et al., 2002. Plant biomass and production and CO2 exchange in an ombrotrophic bog. *Journal of Ecology*, 90 (1), 25–36. doi:10.1046/j.0022-0477.2001.00633.x

Moriasi, D.N., et al., 2007. Model evaluation guidelines for systematic quantification of accuracy in watershed simulations. *Transactions of the ASABE*, 50 (3), 885–900. doi:10.13031/2013.23153

Motovilov, Y.G., et al., 1999. Validation of distributed hydrological model against spatial observations. *Agricultural and Forest Meteorology*, 98-99, 257–277. doi:10.1016/S0168-1923(99)00102-1

Nosent, J. and Bauwens, W., 2012. Application of normalized Nash – sutcliffe efficiency to improve the accuracy of the Sobol sensitivity analysis of a hydrological model. *EGUGA*, 237. Biocode. EGUGA 14.237N

OpenWeather, n.d. Available from: https://openweathermap.org/

Quinton, W.L. and Gray, D.M., 2003. Subsurface drainage from organic soils in permafrost terrain: the major factors to be represented in a runoff model. Proceedings of the 8th International Conference on Permafrost, Davos, Switzerland, 6 pp.

Quinton, W. and Hayashi, M., 2004. The flow and storage of water in the wetland-dominated central Mackenzie river basin: recent advances and future directions. *Prediction in Ungauged Basins: Approaches for Canada's Cold Regions, Canadian Water Resources Association*, 45–66.

Quinton, W.L., Carey, S.K., and Pomeroy, J.W., 2005. Soil water storage and active-layer development in a sub-alpine tundra hillslope, southern Yukon Territory, Canada. *Permafrost Periglacial Process*, 16 (4), 369–382. doi:10.1002/ppp.543

Quinton, W.L. and Baltzer, J.L., 2013. The active-layer hydrology of a peat plateau with thawing permafrost (Scotty Creek, Canada). *Hydrogeology Journal*, 21 (1), 201–220. doi:10.1007/s10040-012-0935-2

Quinton, W., et al., 2019. A synthesis of three decades of hydrological research at Scotty Creek, NWT. Canada. *Hydrology and Earth System Sciences*, 23 (4), 1–25. doi:10.5194/hess-23-1-2019

Ramanarayanan, T.S., et al., 1997. Using APEX to identify alternative practices for animal waste management. ASAE Paper No. 972209. St. Josepth, Mich: ASAE.

Reeve, A.S., Siegel, D.I., and Glaser, P.H., 2000. Simulating vertical flow in large peatlands. *Journal of Hydrology*, 227 (1–4), 207–217. doi:10.1016/S0022-1694(99)00183-3

Ritter, A. and Munoz-Carpena, R., 2013. Performance evaluation of hydrological models: statistical significance for reducing subjectivity in goodness-of-fit assessments. *Journal of Hydrology*, 480, 33–45. doi:10.1016/j.jhydrol.2012.12.004

Ritter, A. and Munoz-Carpena, R., 2020. *FITEVAL* [online]. University of Florida, IFAS Research. https://abe.ufl.edu/faculty/carpena/software/FITEVAL.shtml

Shi, X., et al., 2015. Representing northern peatland microtopography and hydrology within the community land model. *Biogeoscience*, 12 (21), 6453–6477. doi:10.5194/bg-12-6463-2015

SoilGrid REST, n.d. Available from: https://rest.isric.org/

Sonnentag, O., et al., 2008. Spatially explicit simulation of peatland hydrology and carbon dioxide exchange: influence of mesoscale topography. *Journal of Geophysical Research – Biogeosciences*, 113 (G2). doi:10.1029/2007JG000605

Strack, M., et al., 2006. Response of vegetation and net ecosystem carbon dioxide exchange at different peatland microforms following water table drawdown. *Journal of Geophysical Research*, 111 (G2), G02006. doi:10.1029/2005JG000145

Sulman, B.N., et al., 2009. Contrasting carbon dioxide fluxes between a drying shrub wetland in Northern Wisconsin, USA, and nearby forests. *Biogeosciences*, 6 (6), 1115–1126. doi:10.5194/bg-6-1115-2009

Talbot, J., et al., 2014. Increases in abovefround biomass and leaf area 85 years after drainage in a bog. *Botany*, 92 (10), 713–721. doi:10.1139/cjb-2013-0319

Thien, S.J. and Graveel, J.G., 2003. *Laboratory manual for soil science: agricultural & environmental principles*. Preliminary. Dubuque, Iowa 52002: Kendall/Hunt Publishing Company.

Wallage, Z.E. and Holden, J., 2011. Near-surface macropore flow and saturated hydraulic conductivity in drained and restored blanket peatlands. *Soil Use and Management*, 27 (2), 247–254. doi:10.1111/j.1475-2743.2011.00336.x

Wang, J., Lee, W.F., and Ling, P.P., 2020. Estimation of thermal diffusivity for greenhouse soil temperature simulation. *Applied Sciences*, 10 (2), 653. doi:10.3390/app10020653

Weber, T.K.D., Iden, S.C., and Durner, W., 2017. A pore-size classification for peat bogs derived from unsaturated hydraulic properties. *Hydrology and Earth System Sciences*, 21 (12), 6185–6200. doi:10.5194/hess-21-6185-2017

Weiss, R., et al., 2006. Simulation of water table level and peat temperatures in boreal peatlands. *Ecological Modelling*, 192 (3–4), 441–456. doi:10.1016/j.ecolmodel.2005.07.016

Willmott, C.J., 1981. On the validation of models. *Physical Geography*, 2 (2), 184–194. doi:10.1080/02723646.1981.10642213

Willmott, C.J., 1982. Some comments on the evaluation of model performance. *Bulletin of the American Meteorological Society*, 63 (11), 1309–1313. doi:10.1175/1520-0477(1982)063<1309:SCOTEO>2.0.CO;2

Wright, N., Hayashi, M., and Quinton, W.L., 2009. Spatial and temporal variations in active layer thawing and their implication on runoff generation in peat-covered permafrost terrain. *Water Resources Research*, 45 (5), W05414. doi:10.1029/2008WR006880

Xu, J., et al., 2018. PEATMAP: refining estimates of global peatland distribution based on a meta-analysis. *Catena*, 160, 134–140. doi:10.1016/j.catena.2017.09.010

Yu, Z.C., et al., 2003. Carbon sequestration in western Canadian peat highly sensitive to Holocene wet-dry climate cycles at millennial timescales. *The Holocene*, 13 (6), 801–808. doi:10.1191/0959683603hl667ft

Yu, Z.C., 2012. Northern peatland carbon stocks and dynamics: a review. *Biogeosciences*, 9 (10), 4071–4085. doi:10.5194/bg-9-4071-2012